AD A101208

LEVEL II

DEPARTMENT OF THE AIR FORCE
AIR UNIVERSITY (ATC)

AIR FORCE INSTITUTE OF TECHNOLOGY

DTIC
ELECTE
JUL 1 0 1981
S   D
A

Wright-Patterson Air Force Base, Ohio

81 6 30 030

AFIT/GE/EE/80D-41

RE: Distribution Unlimited, Classified
Reference-
No change per Dr. Fontana, AFIT/Elec-
tronics Dept.

⑥ INVESTIGATION OF TERRAIN BOUNCE

ELECTRONIC COUNTERMEASURE.

⑪ Dec 84

⑨ Master's THESIS

⑭ AFIT/GE/EE/80D-41 ⑩ Nancy C. Strasser
Capt USAF

⑫ 105

DTIC
ELECTED
JUL 1 0 1981

A

012225

INVESTIGATION OF TERRAIN BOUNCE ELECTRONIC COUNTERMEASURE

THESIS

Presented to the Faculty of the School of Engineering

of the Air Force Institute of Technology

Air University

in Partial Fulfillment of the

Requirements for the Degree of

Master of Science

by

Nancy C. Strasser, B.S.

Capt   USAF

Graduate Electrical Engineering

December 1980

Acknowledgments

I would like to thank my advisor, Major A. Golden, for the extensive guidance and assistance he has provided. Thanks are also extended to Lt. Col. R. Carpinella, and Capt. P. Rustan, for the reference materials and advice they have provided. Special thanks go to my husband Bob, for his continued support and encouragement.

Contents

List of Figures

List of Symbols

BW	Doppler Bandwidth of missile (Hz)
c	Velocity of light
F	Gain due to shifting direct path signal out of Doppler Bandwidth
F_g	Doppler spread due to amplitude variation (from one terrain facet to another) of reflected signal (Hz)
f_c	Center frequency of missile Doppler Bandwidth (Hz)
f_{jo}	Jammer Doppler offset (optimum)
f'_{jo}	Jammer Doppler offset (sub-optimum)
f_{max}	Maximum Doppler offset of reflected signal
f_{min}	Minimum Doppler offset of reflected signal
f_o	Frequency offset (of reflected signal from direct path signal)
f_t	Original transmit frequency
ΔF_i	Doppler spread of reflected signal over a patch of reflecting terrain
ΔF_j	Jammer Doppler spreading
ΔF_s	Required Doppler spreading (optimum)
$\Delta F'_s$	Required Doppler spreading (sub-optimum)
ΔF_t	$f_{max} - f_{min}$
G_a	$G_{jg}G_{mg}/G_{jm}G_{mj}$
G_{jg}	Gain of jammer in direction of ground
G_{jm}	Gain of jammer in direction of missile
G_r	Gain of repeater
G_{ra}	Gain of ground radar in direction of aircraft
G_t	G_{jm}/G_{jg}
$g(\theta)$	Antenna pattern
H_r, H_t	Altitude of receiver and target (meters)
$(J/S)_s$	System Jamming to Signal Ratio
K	$((R_{mg}+R_{ga})/R_{ma})^2$
K_{pd}	Phase detector constant
L_a	Loss due to absorption by terrain
L_s	Loss due to Doppler spreading of signal
P_d	Direct path power received at missile
P_i	Indirect (reflected) path power received at missile
P_t	Transmit power
R	Ground range from transmitter to receiver $= x_1 + x_2$

R_{ai}	Distance from aircraft to projected point of intercept
R_c	Critical range
R_{ga}	Distance from ground point to aircraft
R_{gi}	Distance from ground point to projected point of intercept
R_{ma}	Distance from missile to aircraft
R_{mg}	Distance from missile to ground point
R_{mi}	Distance from missile to projected point of intercept
R_{ra}	Distance from ground radar to aircraft
R_{rm}	Distance from ground radar to missile
$\dot{R}_{ga}$	Range rate between ground point and aircraft
$\dot{R}_{ma}$	Range rate between missile and aircraft
$\dot{R}_{mg}$	Range rate between missile and ground point
$\Delta \dot{R}$	Difference between direct path and indirect path range rates
T	Horizontal correlation distance
V_1, V_2	Voltage signals from true target and false target
$\vec{v}_a$	Velocity of aircraft
$\vec{v}_m$	Velocity of missile
v_{pd}	Tracking voltage (at phase detector)
x, x_1	Ground distance from receiver to point on terrain
x_2	Ground distance from point on terrain to target
y	Width of glistening area
α	Slope of elementary surface mirror
α_1	Angular distance between true target and power centroid
α_2	Angular distance between false target and power centroid
β	Angle made by bisector of angles of incidence and reflection with the vertical
β_o	rms slope of surface facets
γ	Angle between $\vec{v}_m$ and $-\hat{x}_{mg}$
ζ^2	$(V_1/V_2)^2$ = Effective J/S
η	Angle between $\vec{v}_a$ and $\hat{x}_{ga}$
θ	Angular distance between true target and power centroid
θ_a	Angle of attack from missile to aircraft
θ_{ma}	Angle between line of sight (from missile to aircraft) and the horizontal
θ_{res}	$\Delta \theta$ at which tracker resolves two equal power targets
θ_{size}	Angular size of ground patch

θ_s	Squint angle
θ_{3a}	3-dB beamwidth of jammer antenna
θ_{3m}	3-dB beamwidth of missile antenna
$\Delta\theta$	Angular distance between true target and false target
λ	Wavelength
ρ^2	Terrain reflection coefficient
ρ_d^2	Diffuse reflection coefficient
σ_h	rms surface height variation
σ^0	Bistatic scattering coefficient
σ_t	Target (aircraft) cross-section
ψ	Angle between $\vec{v}_a$ and $\hat{x}_{ma}$
ϕ	Angle between $\vec{v}_m$ and $-\hat{x}_{ma}$
ψ_r	Receive angle (from horizontal) $= \mathrm{Tan}^{-1}(H_r/x_1)$
ψ_t	Transmit angle (from horizontal) $= \mathrm{Tan}^{-1}(H_t/x_2)$

AFIT/GE/EE/80D-41

Abstract

"Terrain Bounce" is an electronic countermeasure intended to defeat
Amplitude Comparison Monopulse Tracking. In this paper the counter-
measure technique is described and its theoretical basis is developed.
The two-target tracking problem, the Doppler offset and spreading of the
ground-reflected signal, and a model for reflection from rough terrain
are presented. A methodology is developed for analyzing the Terrain
Bounce problem. The theory is applied to a typical Terrain Bounce
geometry, and the resulting jammer requirements are derived.

x

I. Introduction

Background

"Terrain Bounce" is an electronic countermeasure intended to defeat Amplitude Comparison Monopulse tracking. The countermeasure is based upon the creation of a false radar target by illuminating the ground with a jamming signal. The purpose of this study is to establish a method for analyzing the Terrain Bounce problem in order to determine the jammer requirements for an assumed problem geometry.

The Terrain Bounce problem geometry is shown in Figure 1. R is the ground range between the missile and the target aircraft; H_t and H_r are the altitudes of the transmitter (aircraft) and receiver (missile); θ_{ma} is the angle made by the line of sight (between the missile and the aircraft) with the horizontal; R_{rm}, R_{ra}, and R_{ma} are the distances from the ground radar to missile, radar to aircraft, and missile to aircraft. R_{mg} and R_{ga} are the distances from the missile to the ground patch, and from the ground patch to the aircraft. It is assumed that the threat is a semi-active missile which detects in Doppler and uses an Angle Amplitude Comparison Monopulse system. The jammer is assumed to be a repeater which receives a signal from the radar and re-radiates it towards the ground. The terrain reflects a portion of the signal back towards the missile, thus creating a false target. The presence of the false target causes missile tracking errors. It is desired to cause a large enough tracking error that the missile is either driven into the ground, or is driven so far off target that it misses.

The success of the countermeasure depends upon the jammer's ability to create a false target at the correct frequency and in an appropriate location to cause errors in tracking. Thus, it depends upon the terrain's

1
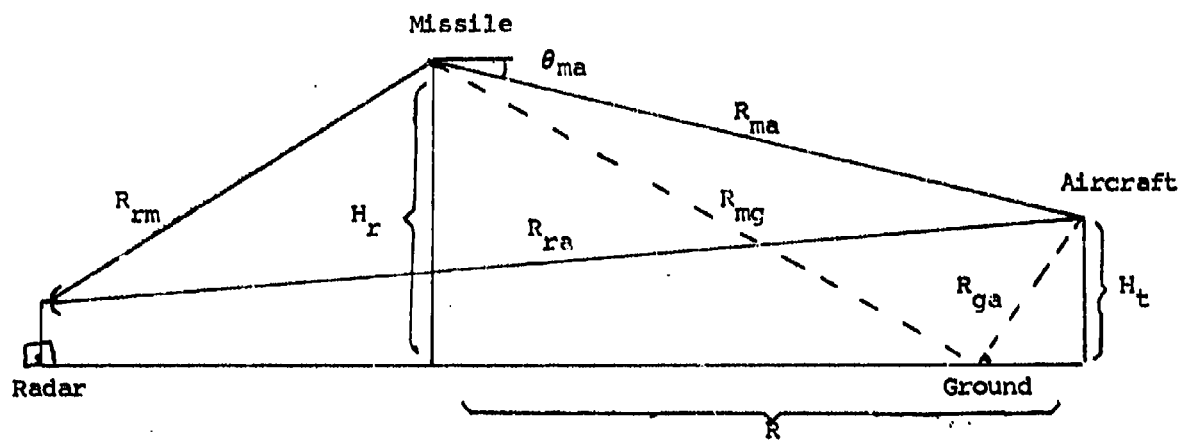
Figure 1. Terrain Bounce Geometry

reflective properties. Reflection from terrain has been the subject of a great deal of investigation. Different authors have variously modeled rough scattering surfaces as perfectly reflecting mirrors (Reference 7), arbitrary protuberances (Reference 25), point scatterers (Reference 23), corrugation (Reference 2) or a composite of these features (Reference 6), in order to determine a reflection coefficient or scattering coefficient. The model developed by Beckmann and Spizzichino (Reference 7) proved to be the most readily adaptable to the Terrain Bounce problem, since it models the surface reflection properties for fixed geometries (transmitter at one point, and receiver at another point). This model was chosen for use in the analysis, and will be further described in Section II.

Scope

This paper presents the theoretical requirements for successful Terrain Bounce jamming. A methodology is developed for analyzing a Terrain Bounce situation, given a particular problem geometry. A detailed example is presented to illustrate the methodology for missile approach from the forward hemisphere.

Approach

The ground reflection is assumed to be diffuse, and the false target is considered as a point target located beneath the ground. In Section II the two-point target tracking problem is developed, and the resulting tracking errors are derived. Next, consideration is given to the Doppler shift and spreading which affect the ground-bounced signal. A model for the terrain is presented and applied to the Terrain Bounce situation. Finally, a methodology is presented for analyzing a Terrain Bounce problem. In Section III, the methodology is applied to a particular problem geometry in order to determine the circumstances under which the countermeasure

3

will be effective, and the requirements on the jammer (jamming beam orientation and beamwidth, Jamming-to-Signal Ratio (J/S), antenna side-lobe levels, and required Doppler offset and spreading of the jamming signal). Section IV presents conclusions, and recommendations for further investigation.

II. Theory

Analysis of Terrain Bounce Countermeasure

The Terrain Bounce problem will be analyzed as a two-point tracking problem, assuming both the true target (aircraft) and the false target to be point targets. The false target is created by illuminating a patch on the ground which reflects a signal towards the missile. Ideally, the reflecting point may be replaced by an image of the source located beneath the ground. (See Figure 2a.) The signal from the image point will differ in Doppler frequency from the direct path signal from the target.

For a realistic surface, the reflection comes from a finite-sized patch, rather than from a single point. Thus the reflected signal will be spread in Doppler over a range of frequencies. Furthermore, reflection occurs at angles other than the specular angle. Thus, the reflecting ground patch may be replaced with a "diffuse image" located beneath the ground (as in Figure 2b), displaced from the "specular image" point. The power centroid of the diffuse image defines the False Target.

There is usually some uncertainty in the problem geometry (missile speed and direction of approach unknown), which creates a requirement for spreading of the reflected signal. Thus, the Doppler spreading of the reflected signal, mentioned above, can be utilized to advantage. The difference between the required spreading and that provided by the terrain-reflected signal must be provided by the jammer.

A model for reflection from rough terrain (Reference 7: Chapter 12) provides information about the magnitude and location of the reflection to be expected from the terrain. This model provides the reflection characteristics of the False Target (the diffuse image point).

These theoretical concepts are developed in this Section, and will be applied to a Terrain Bounce problem in Section III.

(a) Specular Image Point

(b) "Diffuse Image" Point
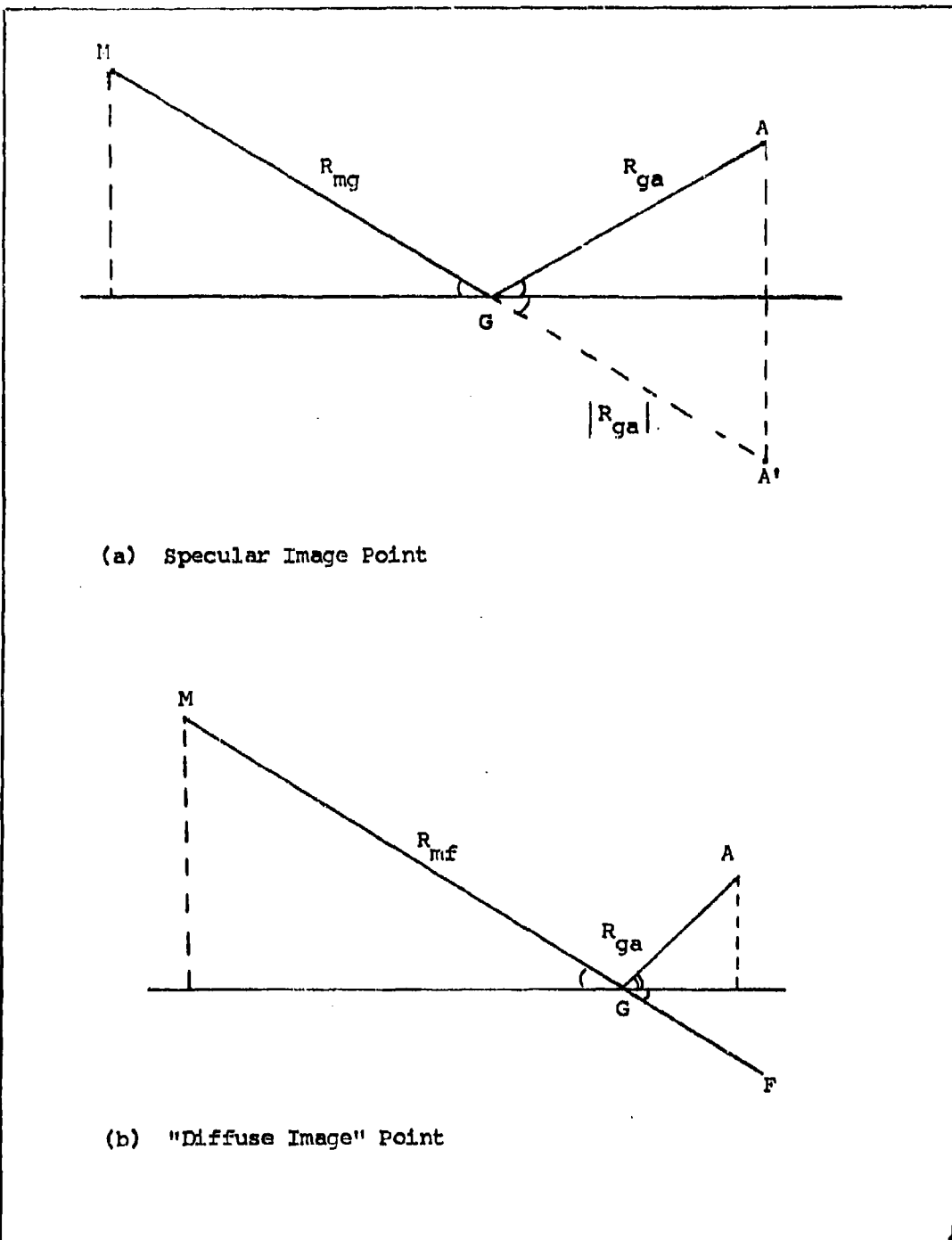
Figure 2. Model for Two-Point Jamming

6

Two-Point Jamming of Monopulse

The first problem to be examined is the influence of two point jamming on the missile tracking. This problem shows the theoretical roots of the Terrain Bounce Countermeasure. In this analysis, the false target will be assumed to be a point source located beneath the ground. (See Figure 2b.) The reflection from the ground will be represented by a constant reflection coefficient times the signal incident upon the ground.

The influence of two incoherent point sources on an Amplitude Comparison Monopulse System with simultaneous comparison of signals has been examined by Vakin and Shustov (Reference 26: Chapter 4). Figure 3 shows the geometry of the problem. The two point sources (the target aircraft A_1, and the false target A_2), are separated by angular distance $\Delta\theta$ and the ratio of their powers is ζ^2. The voltage received by the missile (at the output of the phase detector) is derived in Appendix A, Equation (A-1):

$$v_{pd} = K_{pd}(\zeta^2(g^2(\theta - \theta_s) - g^2(\theta + \theta_s)) + (g^2(\theta - \theta_s - \Delta\theta) - g^2(\theta + \theta_s - \Delta\theta))) \qquad (1)$$

where

$g(\theta) = g_o \exp(-2 \ln 2 (\theta / \theta_{3m})^2)$ for a Gaussian antenna pattern
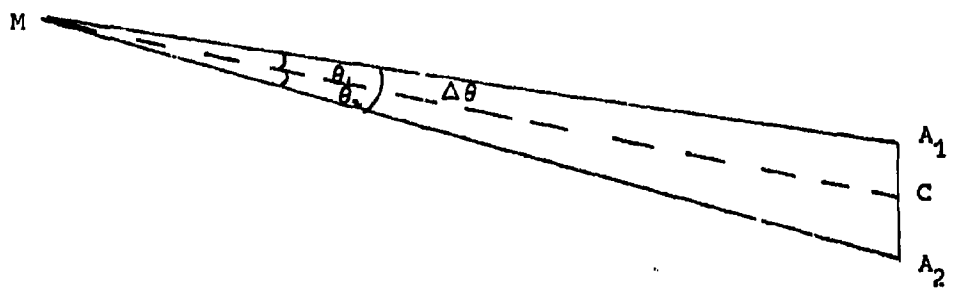
θ_s = squint angle

θ_{3m} = 3-dB beamwidth of missile
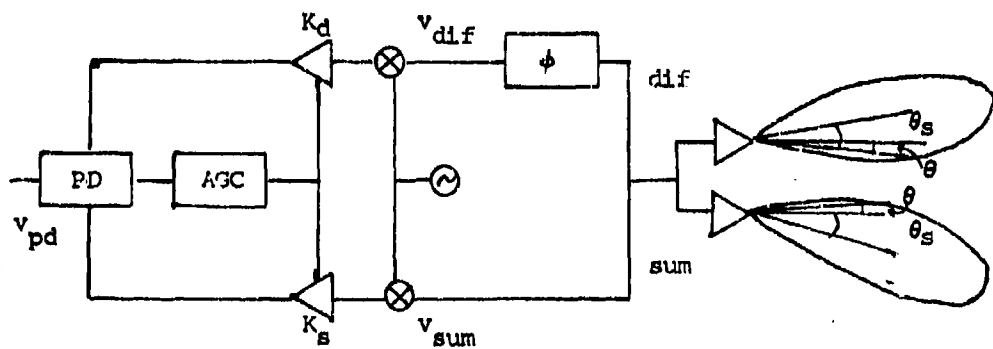
K_{pd} = phase detector constant

θ is measured from source A_1

Equation (1) determines the generalized direction finding characteristic of the system, and may be used to determine the stable tracking points. (Positive slope nulls indicate stable tracking.)

7

(a) Angular Separation of Targets

(b) Squint Angle and Tracking Angle

Figure 3. Two-Point Jamming of Monopulse

8

Figure 4 plots this equation for $K_{pd}=1$ and $\zeta^2=1$ (identical power sources), assuming $\theta_s/\theta_{3m}=.3$. For $\Delta\theta$ small, the system tracks a point midway between the two targets. As $\Delta\theta$ increases, the slope of the v_{pd} curve decreases until, at $\Delta\theta = \theta_{res}$, the slope is equal to zero. ($\theta_{res}=.95\,\theta_{3m}$ in Figure 4). This is the resolution angle, beyond which there are two stable tracking points corresponding to the two targets.

For two targets of unequal power ($\zeta^2 \neq 1$) similar plots indicate that there is no point for which both the slope of the curve and the value of v_{pd} are equal to zero. (See Figure 5 for $\zeta=.5$.) Thus, there is no physical "resolution point"; the system tracks the power centroid, which is located nearer to the more powerful target.

The slope of each curve in Figures 4 and 5 is equal (within a constant factor) to the gain of the transfer function of the direction finder (Reference 26: 195). Thus a decrease in slope (and, hence, in the transfer function of the system) degrades the quality of the transient process and affects the dynamic error.

The parameter θ/θ_{3m} may be interpreted as the tracking error. Figure 6 plots θ/θ_{3m} vs. $\Delta\theta/\theta_{3m}$ for various values of ζ for an assumed Gaussian antenna pattern. As seen in Figure 6, in order to achieve large errors, a small value of ζ is required, (i.e., the false target signal must be stronger than the true target signal). Beyond a certain value of $\Delta\theta/\theta_{3m}$ (the points of discontinuity in Figure 6) there will be two stable tracking points (corresponding to the true target and the false target). Figure 6 indicates that, up to a point, the error will increase with increasing $\Delta\theta$, (i.e., as the missile closes on the targets). For a given antenna pattern function, it is assumed that after $\Delta\theta/\theta_{3m}$ reaches some critical value $(\Delta\theta/\theta_{3m})_{crit}$, the weaker target

9
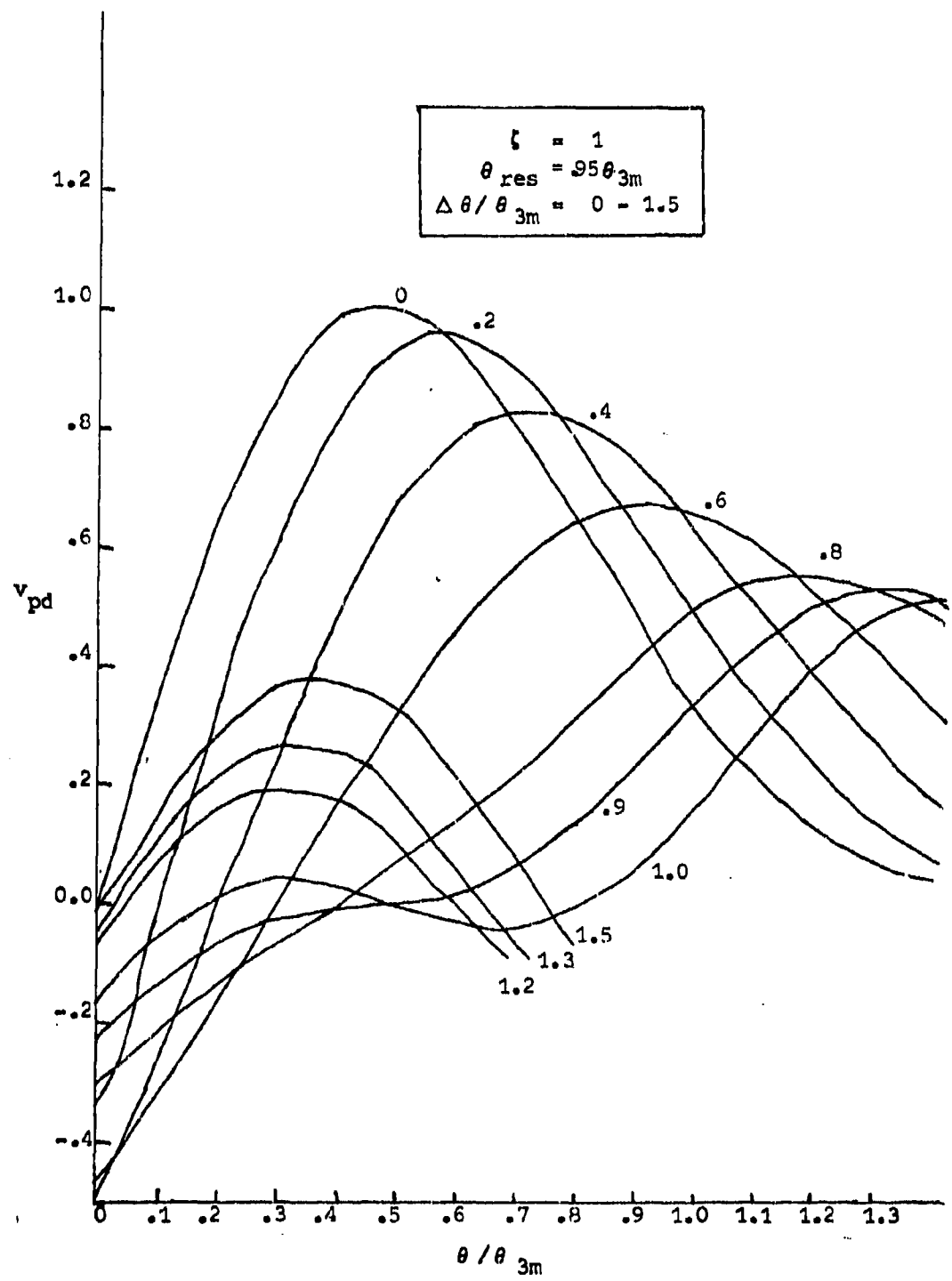
Figure 4. Tracking of Equal Power Targets
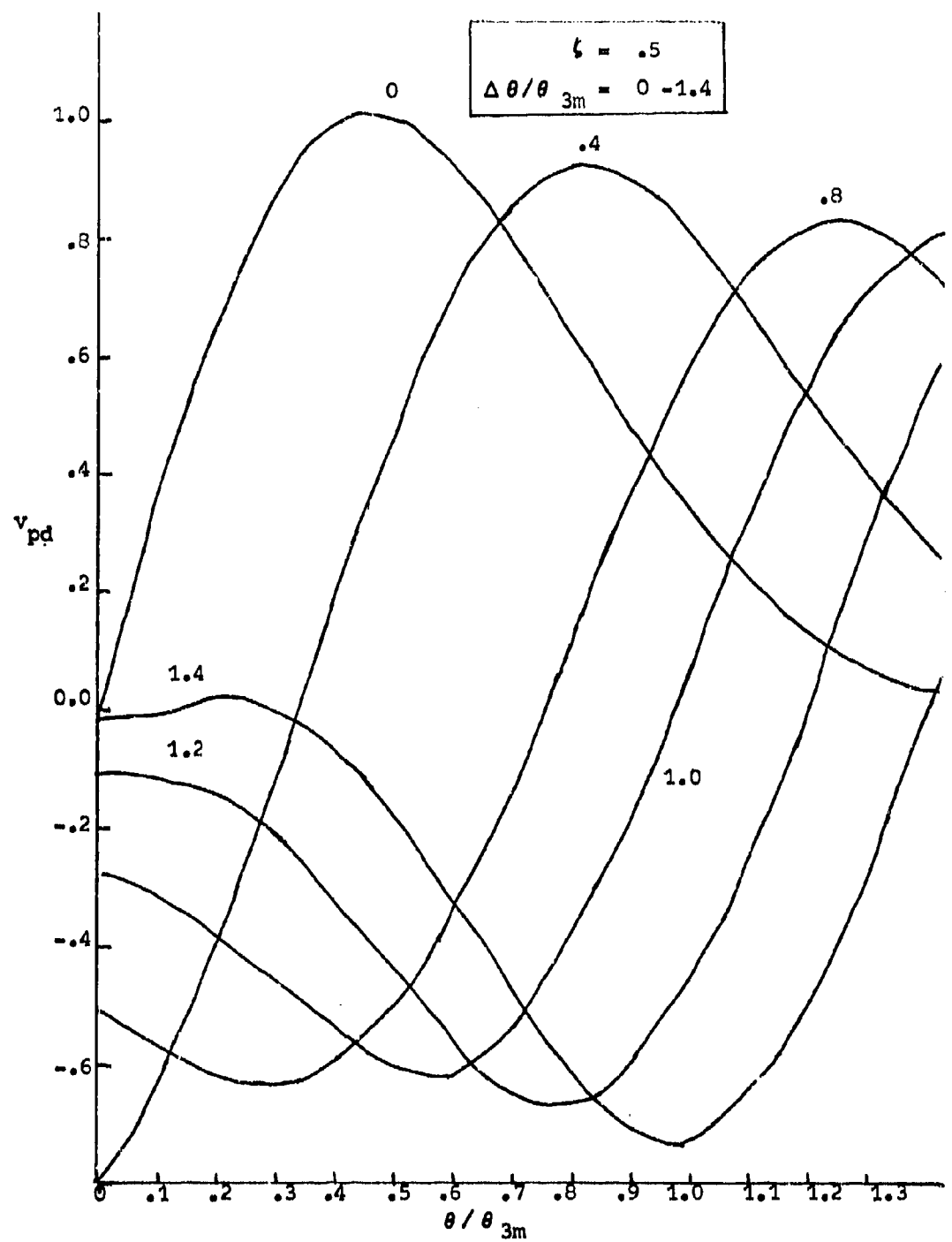
Figure 5. Tracking of Unequal Power Targets
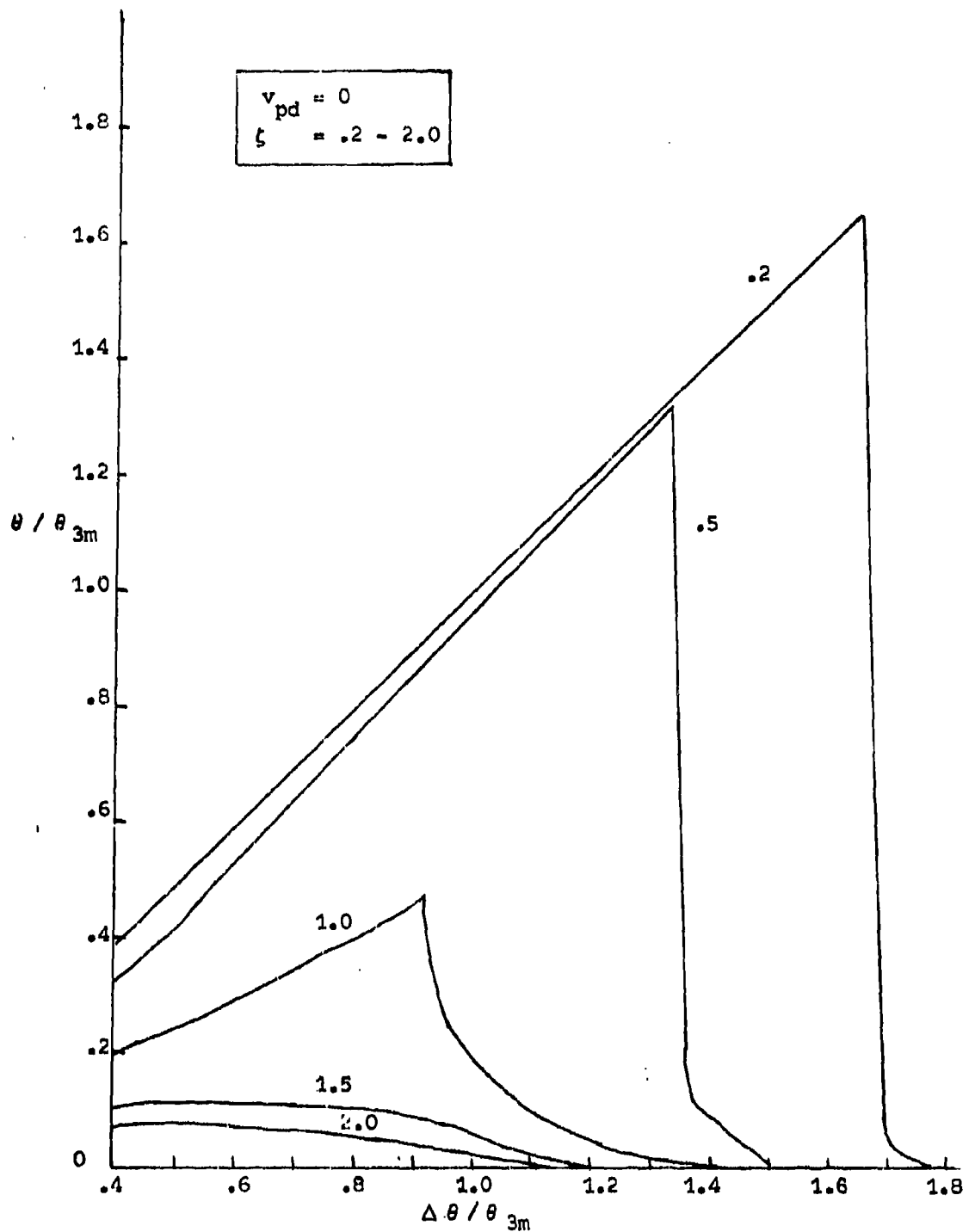
Figure 6. Tracking Error (θ / θ_{3m})

has disappeared from the missile 3-dB beamwidth. Thus, a value of ζ must be selected which will give increasing errors as $\Delta\theta/\theta_{3m}$ approaches and attains $(\Delta\theta/\theta_{3m})_{crit}$. In other words, there must be only one stable tracking point for $\Delta\theta/\theta_{3m} \leq (\Delta\theta/\theta_{3m})_{crit}$.

The quantity $\theta/\Delta\theta$ is a measure of the error away from the true target (A_1). This quantity may be determined by solving Equation (1) for θ, (with $v_{pd}=0$ at the stable tracking point), and normalizing by $\Delta\theta$. Using the derivation in Appendix A (Equation (A-3)), the solution can be found from the transcendental equation:

$$\frac{\zeta^2 + \exp(-4\ln2\,((\Delta\theta/\theta_{3m})^2 - 2(\Delta\theta/\theta_{3m})(\theta/\theta_{3m})))\exp(-8\ln2\,(\Delta\theta/\theta_{3m})(\theta_s/\theta_{3m}))}{\zeta^2 + \exp(-4\ln2\,((\Delta\theta/\theta_{3m})^2 - 2(\Delta\theta/\theta_{3m})(\theta/\theta_{3m})))\exp(+8\ln2\,(\Delta\theta/\theta_{3m})(\theta_s/\theta_{3m}))}$$

$$= \exp(-16\ln2\,(\theta_s/\theta_{3m})(\theta/\theta_{3m})) \qquad (2)$$

The parameter ζ^2 (the ratio of target powers) is the effective Jamming-to Signal Ratio, and is derived in Appendix B, Equations (B-5) and (B-6):

$$\zeta^2 = \left(\frac{V_1}{V_2}\right)^2 = \left(\frac{R_{mf}}{R_{ma}}\right)^2 \left(\frac{(\lambda^2/4\pi)\,G_{jr}G_r G_{jm} + \sigma_t}{(\lambda^2/4\pi)\,G_{jr}G_r G_{jg}\,\rho^2}\right)$$

where

V_1, V_2 = amplitudes of signals from targets A_1 and A_2

R_{ma} = range from missile to aircraft

R_{mf} = range from missile to false target

G_{jr} = gain of jammer in direction of ground radar

G_r = gain of repeater

G_{jg} = gain of jammer in direction of ground

G_{jm} = gain of jammer in direction of missile

13

σ_t = target (aircraft) cross-section

ρ^2 = terrain reflection parameter

λ = wavelength

Assuming that the reflection from the terrain is entirely diffuse, the ratio of the power scattered from the ground to the direct path jammer power is defined as the diffuse reflection coefficient ρ_d^2. It may be seen that $\rho_d^2 = (1/\zeta^2)$ if $\sigma_t = 0$. For an omnidirectional jamming antenna ($G_{jm} = G_{jg}$), this gives $\rho_d^2 = \rho^2 (R_{ma}/R_{mf})^2$. Thus, we obtain:

$$\zeta^2 = \frac{(\lambda^2/4\pi)\, G_{jr} G_r G_{jm} + \sigma_t}{(\lambda^2/4\pi)\, G_{jr} G_r G_{jg}\, \rho_d^2} \tag{3}$$

This equation may be further simplified to:

$$\zeta^2 = \frac{(1/(J/S)_s) + (G_{jm}/G_{jg})}{\rho_d^2} = \frac{(1/(J/S)_s) + G_t}{\rho_d^2} \tag{4}$$

where

$$(J/S)_s = (\lambda^2/4\pi)\, G_{jr} G_r G_{jg}/\sigma_t = \text{System J/S}$$

$$G_t = G_{jm}/G_{jg}$$

Equations (2) and (4) essentially establish the System J/S and antenna sidelobe levels (G_{jm}/G_{jg}) required of the jammer, to obtain the desired miss (given in terms of $\theta/\Delta\theta$).

Doppler Offset

The previous section shows that the success of the Terrain Bounce countermeasure requires that the ground target's signal be more powerful than the true target's signal. To be so, it is necessary that the ground-bounced jamming signal fall within the missile's Doppler Bandwidth.

Assuming the reflecting ground patch to be a point target, some Doppler offset may be required to shift it into the missile's Doppler Bandwidth. If the Doppler Bandwidth is BW Hz wide and is centered at the frequency of the target's skin return (f_c), the ground-bounced signal must be offset in Doppler enough to shift it to within $\pm$ BW/2 Hz of f_c. This offset f_o may be calculated for any point on the ground which reflects the signal towards the missile. If the reflecting ground patch has a finite extent, (rather than being a point source), there are a range of offsets allowed. For any particular finite sized ground patch, this range of offsets will be designated ΔF_i. If multiple problem geometries are to be covered simultaneously by the jammer, various ranges of ΔF_i will be required. The entire range of offsets required for these various ground patches will be designated ΔF_t.

In order to determine the range of Doppler frequency offsets ΔF_t, it is first necessary to determine the offset f_o associated with an arbitrary point on the ground. Figure 7 depicts the generalized aircraft-missile-ground geometry to be considered (Reference 27). $\vec{v}_a$ and $\vec{v}_m$ are the velocity vectors of the aircraft and missile respectively. Using the aircraft as the center of the coordinate system, $\hat{x}_{ma}$ and $\hat{x}_{ga}$ are unit vectors in the directions of the missile and the ground. $\hat{x}_{mg}$ is the unit vector in the direction from the ground to the missile. Considering the aircraft as stationary, the velocities of interest become $\vec{v}_g'$ ($= -\vec{v}_a$), and $\vec{v}_m'$ ($= \vec{v}_m - \vec{v}_a$). Along the direct path between the aircraft and the missile, the range rate is:

$$\dot{R}_{ma} = \hat{x}_{ma} \cdot \vec{v}_m' = \hat{x}_{ma} \cdot (\vec{v}_m - \vec{v}_a) \tag{5}$$

Along the indirect path from the aircraft to ground to missile, the
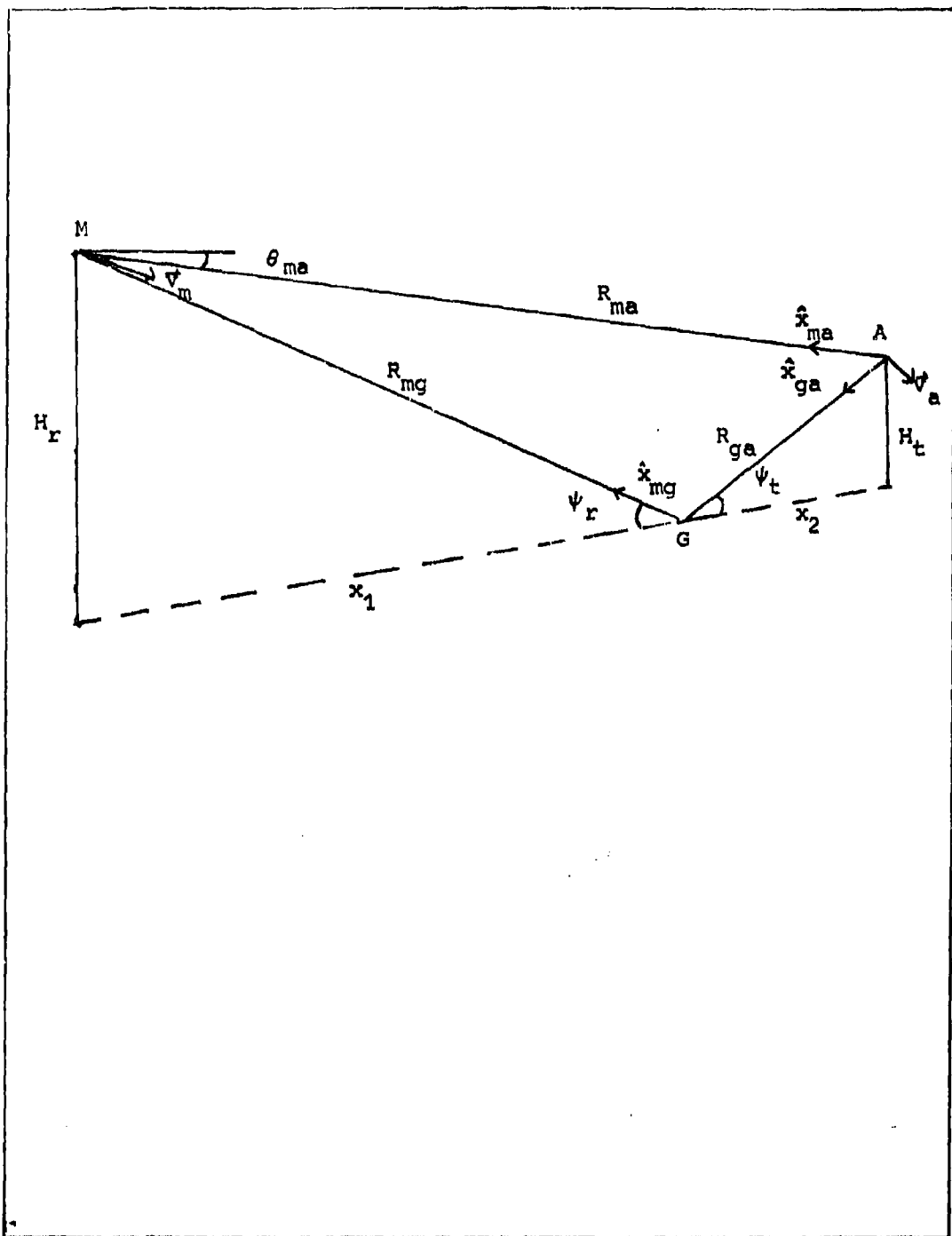
Figure 7. Reflection Path Geometry

range rate is:

$$\dot{R}_{ga} + \dot{R}_{mg} = \hat{x}_{ga} \cdot \vec{v}'_g + \hat{x}_{mg} \cdot (\vec{v}'_m - \vec{v}'_g)$$

$$= -\hat{x}_{ga} \cdot \vec{v}_a + \hat{x}_{mg} \cdot (\vec{v}_m - \vec{v}_a + \vec{v}_a)$$

$$= -\hat{x}_{ga} \cdot \vec{v}_a + \hat{x}_{mg} \cdot \vec{v}_m \qquad (6)$$

The difference between the direct path and some indirect path range rate is given by:

$$\Delta \dot{R} = \dot{R}_{ma} - (\dot{R}_{ga} + \dot{R}_{mg}) = \hat{x}_{ma} \cdot \vec{v}_m - \hat{x}_{ma} \cdot \vec{v}_a + \hat{x}_{ga} \cdot \vec{v}_a - \hat{x}_{mg} \cdot \vec{v}_m \qquad (7)$$

Equation (7) may be rewritten, using the results of Appendix C:

$$\Delta \dot{R} = v_m (\cos \gamma - \cos \phi) + v_a (\cos \eta - \cos \psi) \qquad (8)$$

where the angles are identified in Appendix C as follows:

η = angle between $\vec{v}_a$ and $\hat{x}_{ga}$ = $\cos^{-1} \left(\dfrac{R^2_{ai} + R^2_{ga} - R^2_{gi}}{2 R_{ai} R_{ga}} \right)$

λ = angle between $\vec{v}_m$ and $-\hat{x}_{mg}$ = $\cos^{-1} \left(\dfrac{R^2_{mi} + R^2_{mg} - R^2_{gi}}{2 R_{mi} R_{mg}} \right)$

ϕ = angle between $\vec{v}_m$ and $-\hat{x}_{ma}$ = $\sin^{-1}((v_a / v_m) \sin \psi)$

ψ = angle between $\vec{v}_a$ and $\hat{x}_{ma}$

Here a subscripted value of R indicates the range between two positions: g, a, and m indicate the ground, aircraft, and missile; i indicates the projected point of intercept between missile and aircraft (assuming constant velocities).

At long ranges, $\hat{x}_{ma} \approx \hat{x}_{mg}$, and Equation (7) becomes:

$$\Delta \dot{R} \approx v_a (\cos \eta - \cos \psi) \qquad (9)$$

The Doppler offset required to shift the reflected signal (from any

17

point on the ground) into the missile's Doppler Bandwidth is:

$$f_o = -(f_t/c) \, \Delta \dot{R} = - \, \Delta \dot{R} / \lambda \qquad (10)$$

where

f_t = original transmit frequency
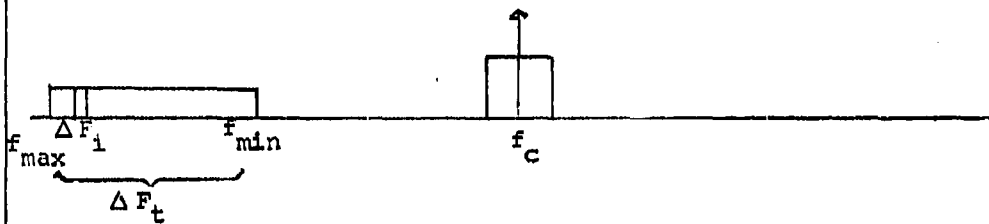
c = velocity of light

An offset of this amount will place the bounced signal (from an
arbitrary point on the ground) at the center of the missile's Doppler
Bandwidth. Thus, Equations (7) or (8), and (10) may be used to calculate
the Doppler difference between the direct path jamming signal and the
signal reflected from any point on the ground. The frequency to be
transmitted by the jammer is $f_t + f_o$.
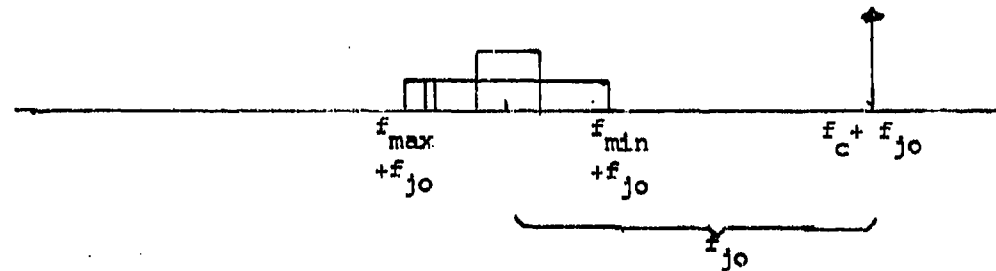
Doppler Spreading

In reality, the ground-bounced signal will be reflected from a
finite-sized ground patch, rather than from a single point. If f_o is
calculated for all of the points in the ground patch, there will be a
range of offsets (ΔF_i) associated with a particular ground patch. In
general, the countermeasure will be designed to utilize one of a number
of possible ground patches, (because of uncertainties in the problem
geometry, to be described later in this section). Thus, the total range
of possible offset frequencies (ΔF_t) includes the ΔF_i's associated
with many different ground patches. (See Figure 8a.)
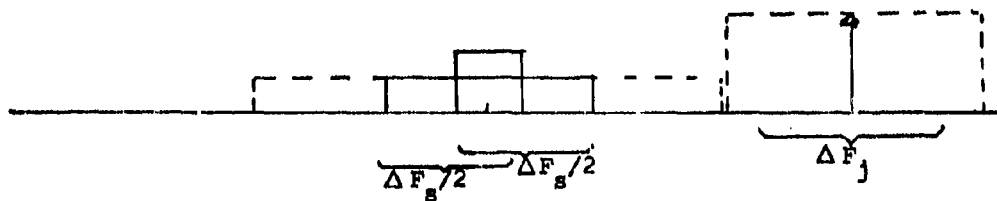
Assuming that this total range of offset values (ΔF_t) is bounded
by f_{min} and f_{max} (see Figure 8a), their total spread in Doppler is
$\Delta F_t = |f_{max} - f_{min}|$. The ΔF_i associated with a particular ground patch
may lie anywhere within this range. Thus, it is desirable to be able
to shift any frequency between f_{min} and f_{max} into the missile's Doppler

18

(a) Range of Doppler frequencies (ΔF_t) of reflected signal which may be available for jamming

(b) Doppler offset of $f_{jo} = (f_{min} + f_{max})/2$ shifts center of ΔF_t to center of Doppler Bandwidth, and shifts direct-path signal out

(c) Spreading of $\Delta F_s = f_{max} - f_{min} + BW = \Delta F_t + BW$ spreads any frequency between f_{min} and f_{max}, such that it may occupy and fill the Bandwidth

Figure 8. Doppler Offset and Spreading - Optimum Case

Bandwidth. If ΔF_t is larger than the missile's Doppler Bandwidth, it is clear that no single jammer offset will place all of these frequencies within the Bandwidth. In order to utilize all frequencies between f_{min} and f_{max} for jamming, each one must be both offset and spread in Doppler.

Assuming that the direct path jamming signal is initially centered in the missile's Doppler Bandwidth (f_c), one may determine the jammer offset (f_{jo}) which will shift the center of ΔF_t to the center of the Bandwidth (as in Figure 8b):

$$f_{jo} = \frac{f_{min} + f_{max}}{2} \qquad (11)$$

Note that, while the center of ΔF_t is shifted to the center of the Doppler Bandwidth, the direct path jamming signal is shifted away from the center of the Bandwidth (and possibly out of the Bandwidth altogether, and into the side-bands). This represents an advantage to the jammer, (since it reduces the direct path signal received by the missile), which should be exploited if at all possible.

Some spreading is also required to insure that either f_{min} or f_{max} (or any frequency in between) may overlap and fill the Bandwidth. (See Figure 8c.) This spreading (ΔF_s) is given by:

$$\Delta F_s = \left| f_{max} - f_{min} \right| + BW = \Delta F_t + BW \qquad (12)$$

where BW is the missile Doppler Bandwidth in Hz. Note that this additional spreading ΔF_s also affects the direct path signal, and care should be taken not to spread it back into the missile Bandwidth. Optimally, f_{jo} and ΔF_s are chosen such that the signal reflected from any ground patch may fall within the missile Bandwidth and the direct path signal may be shifted completely out of the Bandwidth. This

20

amounts to the requirement that:

$$\Delta F_s/2 \leq f_{jo}$$

Using Equations (11) and (12), this gives:

$$\frac{f_{max} - f_{min} + BW}{2} \leq \frac{f_{max} + f_{min}}{2}$$

or,
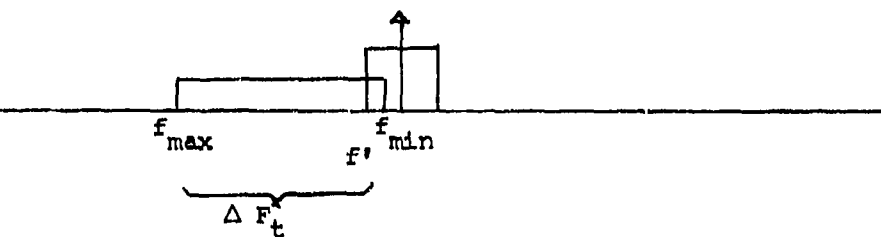
$$f_{min} \geq BW/2 \tag{13}$$

If Equation (13) is not satisfied, then the use of Equations (11) and (12) will allow the direct path signal (after offset and spreading by the jammer) to spread into the missile's Doppler Bandwidth. (See Figure 9a-b.) This condition is highly undesirable, since it allows the direct path jamming to compete more severely with the false target. In order to keep the direct path signal from spreading back into the Doppler Bandwidth, the jammer offset and spreading must be designed to utilize only a portion of the range of frequencies available from the ground. That is, the points which reflect frequencies very close to f_c will not be utilized in the jamming. The sub-optimal parameters f'_{jo} and $\Delta F'_s$ are selected using one or both of the following:
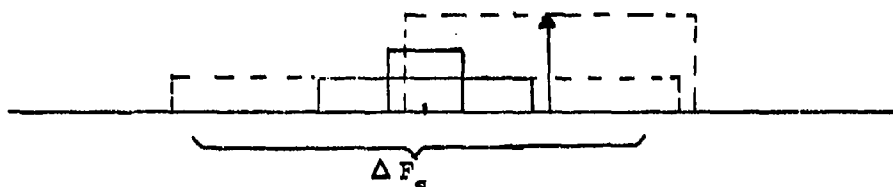
1. Increase f_{jo} (that is, shift only a fraction of the possible terrain-reflected signals into the Doppler Bandwidth)

or,
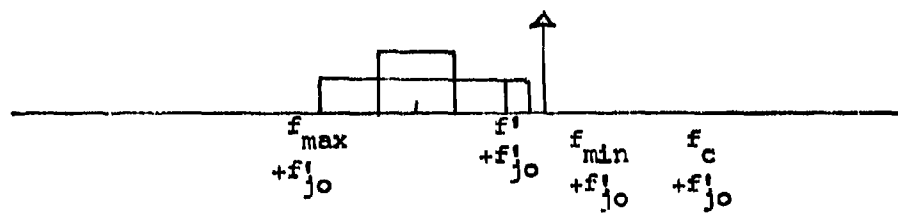
2. Decrease ΔF_s (that is, fill the Doppler Bandwidth partially, instead of completely)

21
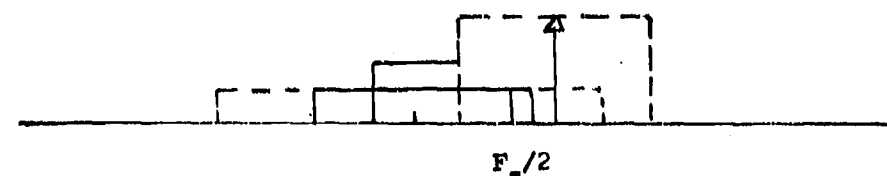
(a) A portion of ΔF_t lies near the frequency of the direct-path jamming signal

(b) Offset by f_{jo} and spreading of ΔF_s shifts the direct-path signal out of the Doppler Bandwidth, but spreads it back into the Bandwidth

(c) Offset by $f'_{jo} = (f_{max} + f')/2$, where $f' \leq BW/2$

(d) Spreading of $\Delta F'_s = 2(f'_{jo} - BW/2) = 2f'_{jo} - BW$ spreads most of the frequencies within ΔF_t such that they may occupy and fill the Bandwidth

Figure 9. Doppler Offset and Spreading - Sub-Optimum Case

This amounts to the requirement (Figure 9c-d) that:

$$f'_{jo} = \frac{f' + f_{max}}{2} \quad , \quad |f'| \geq BW/2 \tag{14}$$

$$\Delta F'_s = 2 (f'_{jo} - BW/2) \tag{15}$$

The penalty for choosing the parameters in this way is the loss of reflection from some ground points which could otherwise contribute to reflection. However, keeping the direct path jamming signal out of the missile's Doppler Bandwidth represents a sizeable advantage for the jammer, which will usually overcome the penalty described above.

ΔF_s (or $\Delta F'_s$) represents the spreading required of the reflected signal. Since the finite-sized ground patch provides some spreading (ΔF_i), the additional spreading required by the jammer is given by:

$$\Delta F_j = \begin{cases} \Delta F_s - \Delta F_i \\ \Delta F'_s - \Delta F_i \end{cases} \tag{16}$$

Using Equation (10), one may calculate the Doppler offset required to shift a signal (reflected from any point on the terrain) into the missile's Doppler Bandwidth. ΔF_t represents the total range of frequency offsets required to make any of the possible reflected signals (from a number of finite-sized reflecting ground patches illuminated by the jammer for different problem geometries) available for jamming. Equations (11) and (12) (or Equations (14) and (15)) give the Doppler offset (f_{jo}) and spreading (ΔF_s) required of the jammer in order to insure that the signal reflected from any point on the terrain may fall within the Doppler Bandwidth of the missile. Equation (16) gives the additional spreading (ΔF_j) which must be provided by the jammer in order to obtain the spreading ΔF_s.

23

Glistening Area Model. Thus far, the properties of the reflected signal have been analyzed. It is now necessary to determine what points on the ground will reflect the jamming signal in the direction of the missile, and how much reflection may be expected. The model for rough terrain which was chosen for this analysis was developed by Beckmann and Spizzichino (Reference 7: Chapter 12). The model does not account for shadowing of portions of the terrain by very large surface irregularities, or for multiple scattering from the surface.

Rough terrain may be modeled as a reflecting surface consisting of elementary mirrors of slope α. The probability distribution of slopes is assumed to be Uniform for $|\alpha| < \alpha_{max}$, where α_{max} is the maximum slope of any mirror. The angle β is made by the bisector of the angles of incidence and reflection with the vertical. The field at the point of reception is caused by those of the elementary mirrors for which the normal to the surface bisects the angle between the incident ray and the ray reflected towards the receiver. At these points, $\alpha = \text{Tan}\,\beta \propto \beta$, and $\alpha_{max} = \text{Tan}\,\beta_{max} \approx \beta_{max}$. (See Figure 10.)

$$\alpha = \text{Tan}\,\beta$$
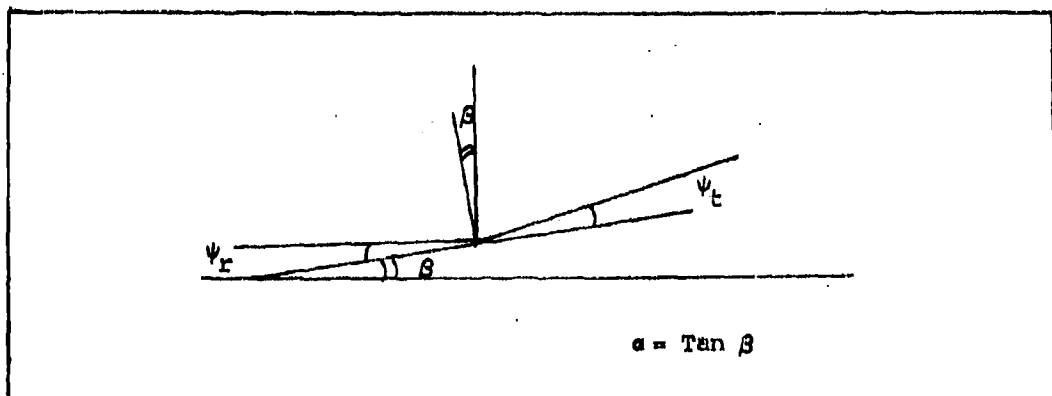
Figure 10. Model of Rough Surface

For a surface illuminated by an omnidirectional transmitter and receiver, the region of the surface for which $|\beta| < \beta_{max}$ participates in reflection for a given position of transmitter and receiver. This area is defined as the "glistening area". The use of directive antennas for the transmitter and receiver may reduce the size of this "glistening area" (if the entire glistening area is not illuminated by the beams). (See Figure 11a.) Thus, the size of the glistening area is determined principally by the irregularities of the reflecting terrain, and secondarily by the antenna patterns. The boundary of the glistening area is determined by finding β in terms of x_1, x_2, and y (Figure 12), and setting $|\beta| = \beta_{max}$ at the boundary. The equation of the glistening area is derived in Appendix D, Equation (D-2). In general, the width of the glistening area (y) as a function of distance x_1 from receiver (Figure 12) is given by:
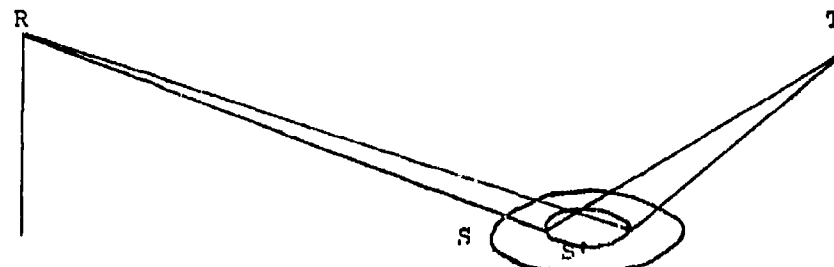
$$\cos \beta_{max} = \frac{1}{b} \left(\frac{H_r}{a_1} + \frac{H_t}{a_2} \right) \tag{17}$$

where

$$a_1 = \sqrt{x_1^2 + y^2 + H_r^2}$$
$$a_2 = \sqrt{x_2^2 + y^2 + H_t^2}$$
$$b = \sqrt{2 + 2(-x_1 x_2 + y^2 + H_r H_t)/a_1 a_2}$$
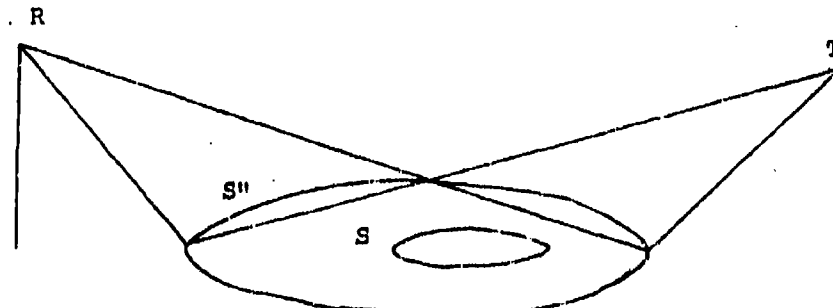
For a given problem geometry and terrain roughness (β_{max}), Equation (17) may be solved iteratively for y, in order to determine the size and location of the glistening area (that is, the area of terrain which participates in reflection towards the receiver). Thus one may determine the area of terrain over which Doppler offset and spreading must be considered.

25

S = Contour of Glistening Area
S'= Contour Illuminated

(a) The use of directive transmit and receive antennas may
     reduce the size of the reflecting ground patch, if they
     do not illuminate the entire glistening area.

S = Contour of Glistening Area
S" = Contour Illuminated

(b) If the antennas illuminate an area larger than the
     glistening area, the area outside the glistening area
     contributes nothing to the reflection towards the
     receiver.

Figure 11. Illumination of Glistening Area by Directive Antennas
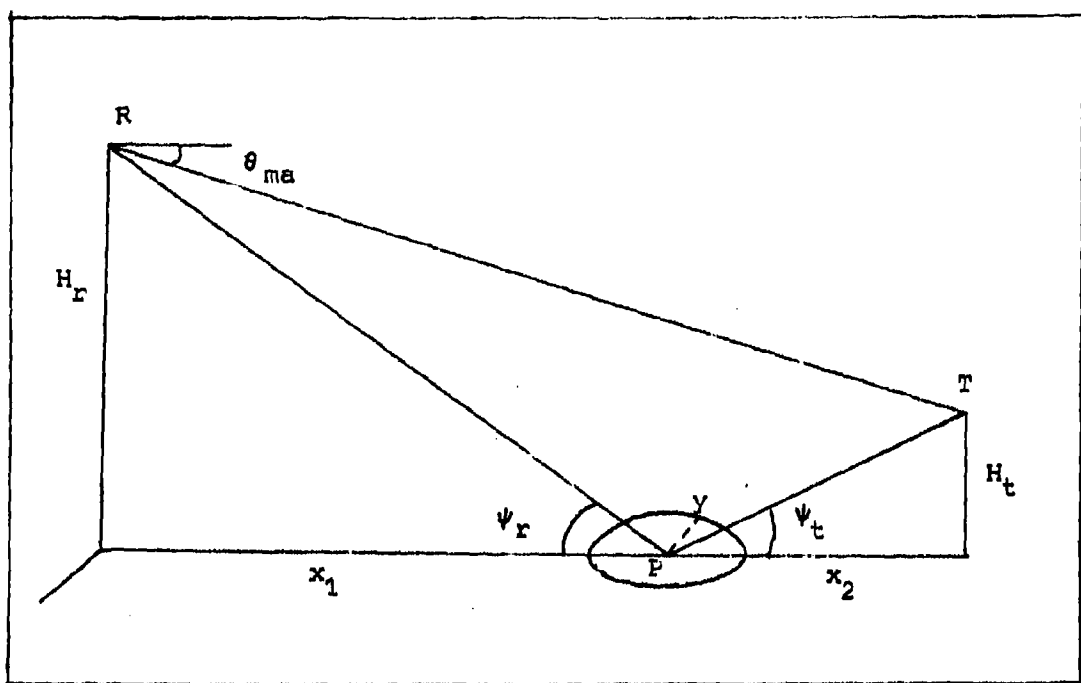
Figure 12. Glistening Area
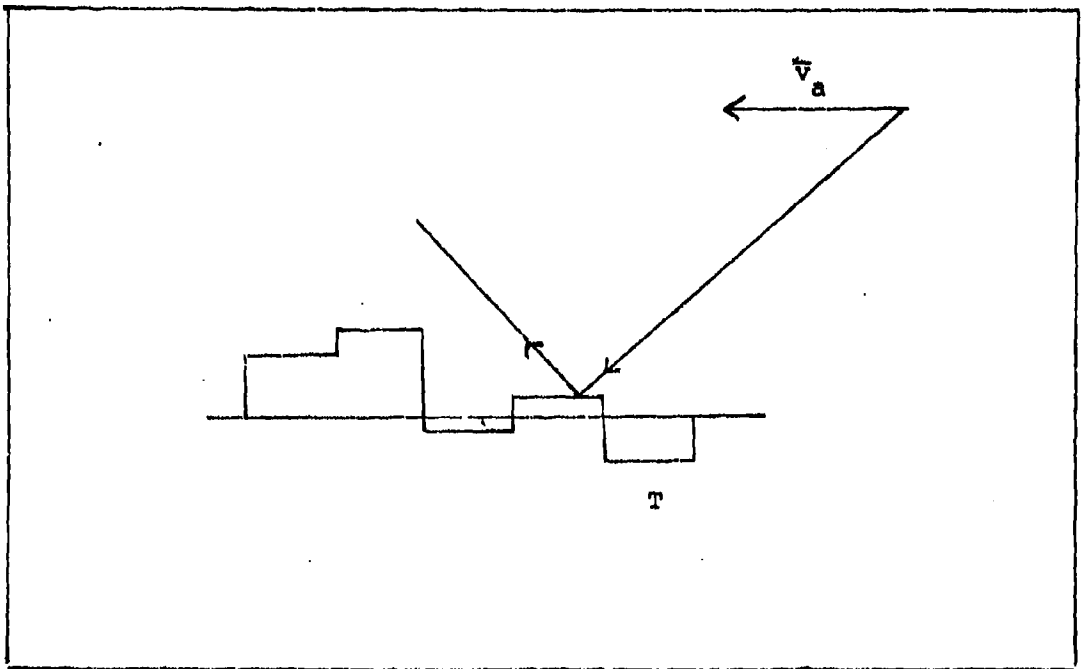
Figure 13. Amplitude Variation across Terrain Facets

Bistatic Scattering Coefficient. The bistatic scattering coefficient (σ°) is a normalized parameter representing radar cross-section per unit area of the surface illuminated. For the Uniform Slope Distribution used in the derivation of the glistening area, the bistatic scattering coefficient is given by Beckmann and Spizzichino (Reference 7: 252-253):

$$\sigma^\circ = G_u(\beta, \beta_{max}) = \begin{cases} \cot^2 \beta_{max} & |\beta| \leq \beta_{max} \\ 0 & |\beta| > \beta_{max} \end{cases} \qquad (18)$$

In general, it is desirable to model the terrain as having a Normal Distribution of irregularities, rather than a Uniform Distribution. For the Normal Distribution, the bistatic scattering coefficient is given by (Reference 7: 252-254):

$$\sigma^\circ = G_n(\beta, \beta_o) = \cot^2 \beta_o \exp(-\tan^2 \beta / \tan^2 \beta_o) \qquad (19)$$

where

β_o = rms slope of facets = $\tan^{-1}(2 \sigma_h / T)$

σ_h = rms surface height variation

T = horizontal correlation distance

In the expression in Equation (19), it is assumed that T is identical for all directions. It is also assumed that the surface is rough enough that the reflection is primarily diffuse and that specular reflection is negligible. Note that the σ° (Equations (18) and (19)) applies to reflection from the glistening area ($|\beta| \leq \beta_{max}$). However, the reported values of σ° are dependent upon measurement technique. To be used in Equations (18) and (19), σ° must be measured over an area which lies entirely within the glistening area. If σ° is averaged over a large area (larger than the glistening area), then it will be averaged

28

over points which do not contribute to the reflection towards the receiver. (See Figure 11b.) Thus, the measurement of σ^0 will be smaller than the theoretical value used here.

For small β ($\ll \beta_o$) Equation (19) is approximately equal to Equation (18), with $\beta_o = \beta_{max}$. Thus, β_o may be used to represent either the maximum or the rms slope of the surface irregularities, and Equation (18) may be used to describe the scattering, except when the detailed scattering behavior at $\beta > \beta_o$ is considered. Furthermore, one may use the glistening area derived for the Uniformly distributed rough surface to approximate that for the Normally distributed rough surface (Reference 3: 690).

Diffuse Reflection Coefficient. (Reference 3). It is now necessary to incorporate this terrain model into the desired reflection parameter of Equation (2) (ρ^2). In this case, it is assumed that the reflection is purely diffuse (negligible specular component), so that ρ^2 in Equation (2) is replaced with the diffuse reflection coefficient ρ_d^2, which is defined as the ratio of the ground-reflected (reflected diffusely from the ground) power received to the direct power received.

The direct power P_d received at the missile is given by:

$$P_d = \frac{P_t \, G_{jm} G_{mj} \, \lambda^2}{(4\pi)^2 \, R_{ma}^2} \tag{20}$$

where

P_t = transmit power

G_{jm} = gain of target (jammer) in direction of receiver (missile)

G_{mj} = gain of receiver in direction of target

R_{ma} = direct path range $\approx R/\cos\theta_{ma}$

The indirect, or terrain-reflected, power P_i received at the missile is given by (Reference 3: 690):

$$P_i = \int_S dP_i = \frac{P_t G_{jg} G_{mg}}{(4\pi)^3} \int_S \frac{\sigma^\circ dS}{R_{ga}^2 R_{mg}^2} \tag{21}$$

where

R_{ga} = distance from target to ground = $x_2/\cos \psi_t$

R_{mg} = distance from receiver to ground = $x_1/\cos \psi_r$

G_{jg} = gain of jammer in direction of ground

G_{mg} = gain of missile in direction of ground

$\sigma^\circ = \sigma^\circ(\psi_t, \psi_r, \phi)$ = bistatic cross-section

ψ_t, ψ_r = grazing angles of incidence and reflection

ϕ = azimuth angle of incidence

dS = element of surface of reflection

S = limits of the surface of reflection

The diffuse reflection coefficient for a small element of surface (over which R_{ga}, R_{mg}, σ°, and the antenna gains are assumed to be constant) is given by (Reference 3: 690):

$$d\rho_d^2 = \frac{dP_i}{P_d} = \frac{G_{jg} G_{mg}}{G_{jm} G_{mj} 4\pi} \left(\frac{R_{ma}}{R_{ga} R_{mg}}\right)^2 \sigma^\circ dS \tag{22}$$

The diffuse reflection coefficient is given by:

$$\rho_d^2 = \frac{G_{jg} G_{mg}}{G_{jm} G_{mj} 4\pi} \int_S \left(\frac{R_{ma}}{R_{ga} R_{mg}}\right)^2 \sigma^\circ dS \tag{23}$$

Using Equation (18) for σ°; the definitions for R_{ma}, R_{ga}, R_{mg};

and $dS=2ydx_1$, we have:

$$\rho_d^2 = \frac{G_{jg}G_{mg}}{G_{jm}G_{mj}2\pi}\frac{R^2}{Tan^2\beta_o Cos^2\theta_{ma}}\int_S \frac{Cos^2\psi_t Cos^2\psi_r\, y\, dx_1}{x_1^2\, x_2^2}$$

$$= \frac{G_a R^2}{2\pi Tan^2\beta_o Cos^2\theta_{ma}}\int_S \frac{Cos^2\psi_t Cos^2\psi_r\, y\, dx}{x^2\,(R-x)^2} \qquad (24)$$

where

$$x = x_1$$
$$R-x = x_2$$
$$G_a = (G_{jg}G_{mg}/G_{jm}G_{mj})$$

It is desirable to evaluate ρ_d^2 over an increment of surface of length Δx, rather than over the entire surface. This gives:

$$\Delta\rho_d^2 = \frac{G_a R^2}{2\pi Tan^2\beta_o Cos^2\theta_{ma}}\int_x^{x+\Delta x}\frac{Cos^2\psi_t Cos^2\psi_r\, y\, dx}{x^2\,(R-x)^2} \qquad (25)$$

$$\rho_d^2 = \Sigma\,\Delta\rho_d^2 \qquad (26)$$

In all of these calculations, it has been assumed that the antenna gains are constant over the 3-dB beamwidth, and may be moved outside the integrals. It will also be assumed that $G_{mg}=G_{ma}$ as long as $\Delta\theta < \theta_{3m}$ (that is, both the target and the ground patch are within the 3-dB beamwidth of the missile), and thereby omit these two parameters from future equations. Further, the jamming antenna will be assumed to be omnidirectional ($G_{jm}=G_{jg}$) for calculation of the glistening area, (in order to obtain the largest terrain patch which contributes to reflection at the receiver). Adjustments will be made for actual antenna pattern in later calculations.

31

Given β_o, θ_{ma}, H_t, and R for a particular geometry, Equation (25) may be solved for $\Delta \rho_d^2$ vs. x (where the range is broken up into intervals of length Δx). For intervals where the glistening area (from Equation (17)) does not exist, there is no contribution to the reflected signal received at H_r. The intervals where the glistening area exists define the ground patch target.

Thus, Equations (25) and (26) may be used to determine the terrain reflection coefficient ρ_d^2, and the position and spatial spread of the reflecting ground patch. These parameters characterize the false target discussed previously.

Additional Doppler Spreading. In addition to the Doppler spreading addressed above (caused by reflection from a finite-sized ground patch, and by additional spreading provided by the jammer), there is also some spreading caused by the amplitude variation (from one facet to another) of the ground-reflected signal. (See Figure 13.) This spreading may be described in terms of the correlation distance T ($= 2 \sigma_h / \mathrm{Tan} \beta_o$). The time required for the aircraft to move across one correlation length T is:

$$t = T/v_a$$

This gives additional frequency spreading on the order of:

$$F_g = v_a/T = v_a/(2 \sigma_h/\mathrm{Tan} \beta_o) \tag{27}$$

Thus an additional spreading of F_g affects the reflected signal. In general, this spreading is negligible compared to the spreading ΔF_t; however, it should be considered if ΔF_t is small (a few hundred Hertz).

Effects of Antenna Directivity

Thus far in the development of the terrain model, it has been

32

assumed that both the receive (missile) and the transmit (aircraft) antennas are omnidirectional. Now, the effects of antenna directivity will be considered. The receive antenna directivity will be used to establish the critical range at which the Terrain Bounce problem can be analyzed, (that is, the range at which the target aircraft is about to disappear from the missile's 3-dB beamwidth). Furthermore, the use of directive antennas will reduce the effective size of the reflecting ground patch, since they will not illuminate the entire glistening area. Thus, the directivity of the transmit antenna may be used to define the location and size of the reflecting ground patch.

Critical Range. Assuming that the receive antenna has 3-dB beamwidth θ_{3m}, it is required that the illuminated ground patch fall within that beamwidth. Furthermore, it is desirable that this condition hold at the range where the target (aircraft) is about to disappear from the missile's 3-dB beamwidth. Figure 14 indicates the locations of the target aircraft (A), false target (F, whose location is determined by that of the power centroid of the reflecting ground patch), and the power centroid (C), with respect to the missile. The angular separation of the two targets, $\Delta\theta$ (used in Equation (2)), is given by:

$$\Delta\theta = \alpha_1 + \alpha_2$$

As the missile approaches the targets, $\Delta\theta$ increases to a point where it exceeds the 3-dB beamwidth of the missile antenna. Beyond this point, the target which is further from the power centroid will be assumed to disappear from the main beam. The range at which this occurs will be called the critical range R_c. Assuming that θ_{3m} is 20° and that the beam is centered on the power centroid (C in Figure 14), the critical
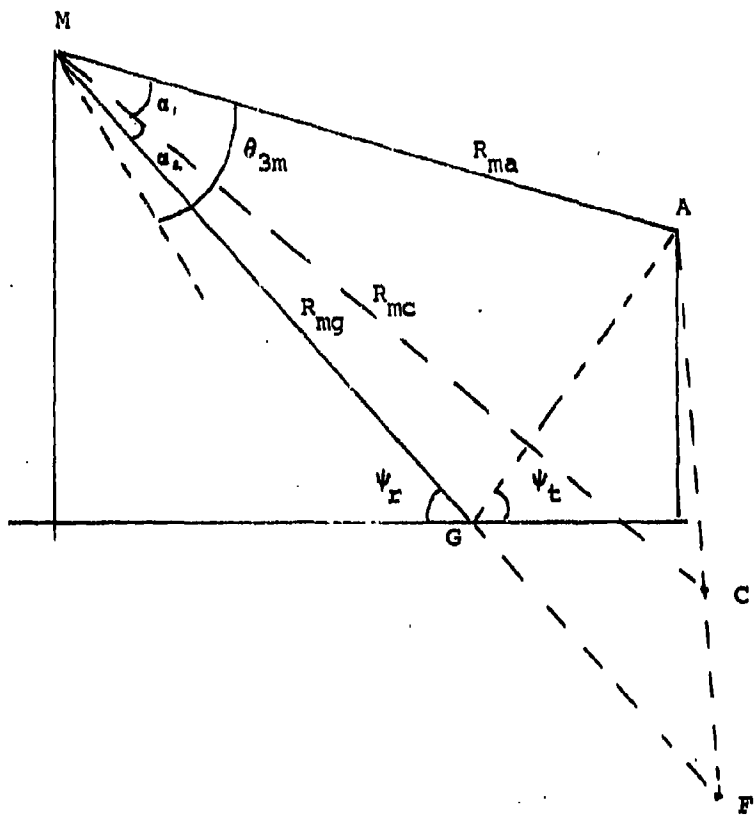
Figure 14. Geometry for Directive Receive Antenna

range occurs when:

$$\alpha_1 = .5 \ \theta_{3m} = 10^{\circ} = .1745 \text{ rad} \tag{28}$$

It is required that the power centroid be closer to the ground than to the aircraft. This leads to the requirement that:

$$\alpha_2 \ll 10^{\circ} \tag{29}$$

The value $\alpha_2 = .05$ rad is chosen in order to provide $\alpha_1 \gg \alpha_2$.

From Figure 12, $\psi_r = \theta_{ma} + \alpha_1 + \alpha_2$, where ψ_r is the receive angle. For $\alpha_1 = .1745$ rad, $\alpha_2 = .05$ rad, the requirement is:

$$\psi_r = \theta_{ma} + .2245 \text{ rad} \tag{30}$$

For a given value of θ_{ma}, and H_t, the critical range R_c is the range at which the power centroid of the glistening area (considered as a point target) satisfies Equation (30).

The choice of α_1 and α_2 above will affect the parameters $\Delta\theta / \theta_{3m}$ and $\theta /\Delta\theta$, used in Section II Equation (2). The ratio of the angular seapration of targets to the 3-dB beamwidth of the missile is given by:

$$\Delta\theta / \theta_{3m} = (\alpha_1 + \alpha_2)/\theta_{3m} = .643 \tag{31}$$

The ratio of the error (away from the true target) to the angular separation of targets is given by:

$$\theta /\Delta\theta = \alpha_1/(\alpha_1 + \alpha_2) = .777 \tag{32}$$

These two parameters (used in Equation (2)) will establish the jammer antenna sidelobe requirements and System J/S for a particular value of ρ_d^2.

Effective Size of Ground Patch. Using Equation (17), one may determine the maximum size of the glistening area (y as a function of x), assuming omnidirectional transmit and receive antennas. Depending upon the roughness of the surface, the range, and θ_{ma}, the glistening area may be a very extensive patch or a very small patch. In order to reflect the maximum possible energy to the receiver, the entire glistening area would have to be illuminated by the jammer. However, the use of directive transmit and receive antennas may reduce the effective size of the reflecting ground patch.

If the glistening area covers most of the area between the transmitter and the receiver, a directive transmit antenna will substantially reduce the size of the reflecting ground patch. It is desirable to choose the transmit antenna directivity such that little reflection is lost in this size reduction. It is found that the illumination of an area near the base of the transmitter reflects a large portion of the transmitted signal towards the missile, and that little reflection is lost if the illuminated area is reduced to this spot. Thus, using a plot of $\Delta \rho_d^2$ vs. x (from Equation (25)), the transmit antenna directivity is chosen to illuminate an area which will provide a large return. Then the critical range R_c is determined based upon this reduced-size ground patch.

If the glistening area covers only a small area between the transmitter and the receiver, the selection of the transmit antenna directivity is less subjective. The entire area which will reflect towards the receiver must be illuminated. The critical range R_c is determined based upon the entire reflecting ground patch.

Terrain Bounce Problem

Thus far, the theoretical roots of the Terrain Bounce Countermeasure

36

have been developed. It is now necessary to relate these concepts to the Terrain Bounce problem geometry. For a given problem geometry (see Figure 1), it is necessary to determine the size and location of the reflecting ground patch, the Doppler frequencies (spread) of the reflected signal, and the magnitude of the reflected signal. Then, it is necessary to determine the jammer offset and additional spreading required for effective jamming. The jammer antenna orientation (depression angle and 3-dB beamwidth) required to illuminate the ground patch may be determined, based upon knowledge of the size and location of the ground patch to be illuminated. Finally, the magnitude of the reflected signal, and the location of the reflecting ground patch may be used to characterize the false target (modeled as a point source located beneath the ground), to determine the required jammer antenna sidelobe levels and the System Jamming-to-Signal ratio.
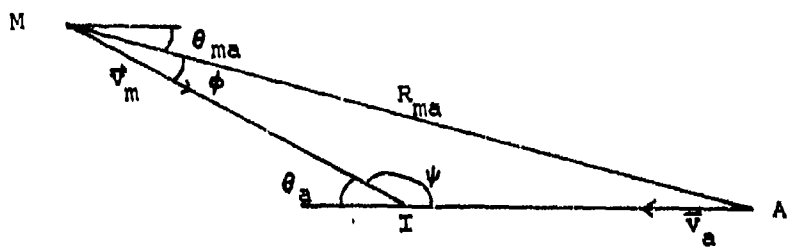
Unfortunately, there are some uncertainties in any problem geometry, since the missile velocity (v_m) and the angle of approach (ψ) are unknown. Rather than solve the Terrain Bounce problem for every possible case, it is possible to examine only a few limiting cases by formalizing the problem uncertainty.

Uncertainties in Problem Geometry. It is assumed that the attack angle from the missile to the aircraft (θ_a from Figure 15), is limited to:
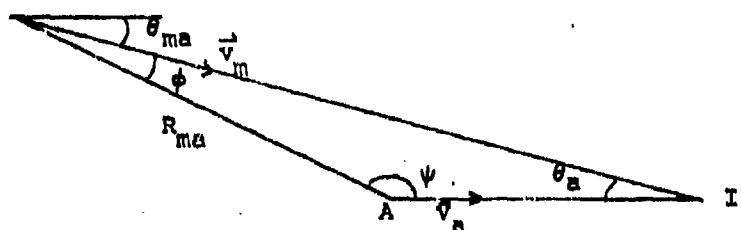
$$5^{\circ} < \theta_a < 35^{\circ} \tag{33}$$

For head-on approach, (see Figure 15a), $\theta_a = \theta_{ma} + \phi$, where $\phi = \sin^{-1}((v_a/v_m)\sin\psi)$, and $\psi = \theta_{ma}$. Thus:
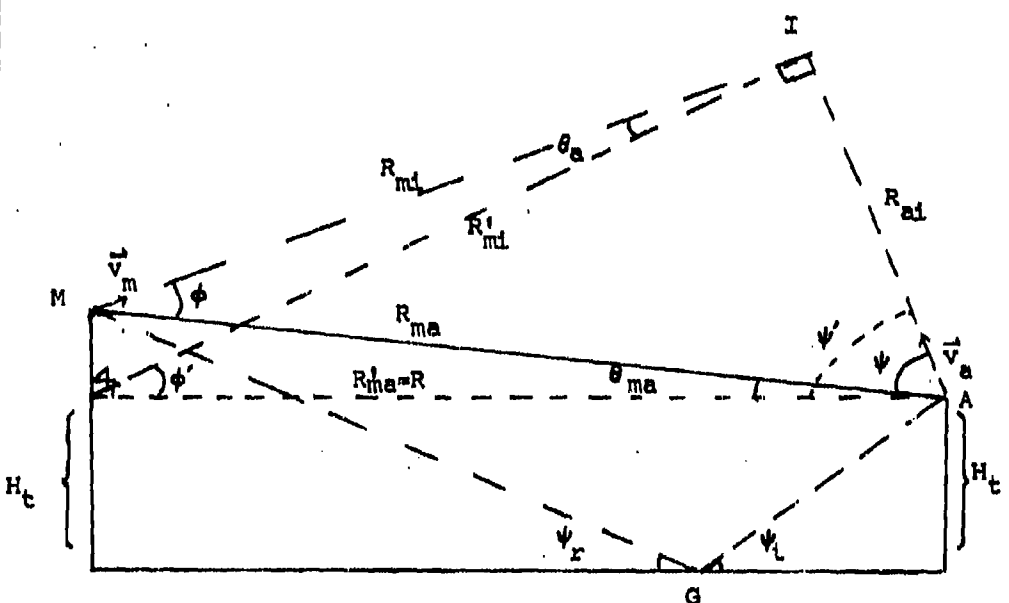
$$\theta_{ma} = \theta_a - \phi = \tan^{-1}\left(\frac{\sin\theta_a}{\cos\theta_a + (v_a/v_m)}\right) \quad \text{(head-on)} \tag{34}$$

37

(a) Head-on Approach

(b) Tail-on Approach

(c) Side-on Approach

Figure 15. Missile Approach to Target

For the case of tail-on approach, (see Figure 15b), $\theta_a = \theta_{ma} - \phi$, and $\psi = 180^\circ - \theta_{ma}$. This gives:

$$\theta_{ma} = \theta_a + \phi = \text{Tan}^{-1}\left(\frac{\sin \theta_a}{\cos \theta_a - (v_a/v_m)}\right) \quad \text{(tail-on)} \quad (35)$$

For side-on approach (path of the missile perpendicular to the path of the aircraft at the point of intercept (see Figure 15c)), we have:

$$\phi + \psi = 90^\circ \quad (36)$$

$$\sin \phi = (v_a/v_m) \sin \psi \quad (37)$$

Equations (36) and (37) must be solved simultaneously for a given v_a and v_m. From Figure 15c we have:

$$\sin \theta_a = a/R_{mi}$$

$$\sin \theta_{ma} = a/R_{ma}$$

$$\sin \psi = R_{mi}/R_{ma}$$

$$\sin \theta_a / \sin \theta_{ma} = R_{ma}/R_{mi} = 1/\sin \psi$$

These relations give:

$$\sin \theta_a = \sin \theta_{ma}/\sin \psi$$

$$\theta_{ma} = \sin^{-1}(\sin \theta_a \sin \psi)$$

Thus, θ_{ma} is bounded by:

$$\sin^{-1}(\sin 5^\circ \sin \psi) < \theta_{ma} < \sin^{-1}(\sin 35^\circ \sin \psi) \quad (38)$$

ϕ is calculated from v_a (known) and v_m, for a range of values of v_m. ($\phi_1 = \phi(v_{min})$, $\phi_2 = \phi(v_{max})$). The larger of the two values is used in Equations (34) and (35) above).

As an example of these calculations, it will be assumed that the aircraft and missile velocities are given by:

$$v_a = 200 \text{ m/sec}$$

$$600 \text{ m/sec} < v_m < 800 \text{ m/sec}$$

Then, Equations (34)-(38) give the following limits on the range of θ_{ma}:

$$4^\circ < \theta_{ma} < 28^\circ \qquad \text{Head-on Approach}$$

$$5^\circ < \theta_{ma} < 34^\circ \qquad \text{Side-on Approach} \qquad (39)$$

$$7^\circ < \theta_{ma} < 50^\circ \qquad \text{Tail-on Approach}$$

Thus, the uncertainties in ψ and v_m are built into the limits on θ_{ma}. The only cases which need be considered are those of head-on approach ($\psi = \theta_{ma}$), tail-on approach ($\psi = 180^\circ - \theta_{ma}$), and side-on approach ($\phi + \psi = 90^\circ$), with $v_m = v_{min}$ and $v_m = v_{max}$ for each case. All possible approach angles and missile velocities fall somewhere between these extremes.

Methodology. It is now possible to translate the theoretical concepts of this section into a systematic methodology for solving a particular Terrain Bounce problem. These steps are:

1. Determine the range of θ_{ma} values required by the uncertainties in v_m and ψ, using Equations (34), (35) and (38). This permits all possible cases (for a particular problem geometry) to be reduced to a few limiting cases.

2. Examine the characteristics of the glistening area ($\Delta \rho_d^2$ vs. x from Equation (25) and ρ_d^2 from Equation (26)) for varying θ_{ma}, ψ, and R. The size of the maximum possible glistening area determines the choice of transmit antenna directivity. If the glistening area is very

40

extensive, the directivity is chosen to illuminate a portion of the ground which reflects a large fraction of the total possible reflected signal towards the receiver. If the glistening area is very small, the directivity is chosen to illuminate the entire ground patch.

3. Establish the critical range R_c for a given θ_{ma} and ψ, using Equation (30). In cases where the glistening area is very extensive, it must be reduced by assuming a jammer antenna depression angle and beamwidth (chosen in Step 2 above). This is the range at which the target aircraft is about to disappear from the 3-dB beamwidth of the missile antenna.

4. Calculate the size and magnitude of the glistening area for θ_{ma}, ψ, and R_c using Equations (25) and (26). The size of the ground patch is used to determine a jamming antenna orientation (if not already selected in Step 2 above). The magnitude of the diffuse reflection coefficient (ρ_d^2) is used to characterize the false target (modeled as a point target beneath the surface of the earth).

5. Calculate the Doppler offset of the ground-bounced signal associated with points on the reflecting ground patch, using Equation (10). These frequencies represent the Doppler spreading which occurs due to the reflection from a finite sized ground patch, rather than a point source. The uncertainty in v_m (used in Equation (8)) further spreads this range of frequencies. The total range of Doppler frequency offsets represents all possible frequencies which may be available for jamming.

These five steps will result in data which is best understood in graphic form. Steps 2-5 are performed for the limiting cases of the problem geometry (defined by the limits on θ_{ma} from Step 1).

The jammer requirements must be determined to cover all possible limiting cases. The jammer requirements which result from this analysis are:

1. The jammer orientation (depression angle and beamwidth) is established in Step 4 above, or by examining the size of the total ground patch which must be illuminated.

2. The required Doppler offset (f_{jo}) and additional spreading (ΔF_j) of the jamming signal is determined from Step 5 above, using Equations (11), (12), and (16).

3. The jammer antenna sidelobe levels (G_{jm}/G_{jg}) and System J/S required to give satisfactory tracking errors are determined using ρ_d^2 (from Step 4) in Equation (2).

III. Application of Theory

Using the methodology presented in Section II, one may, for a given problem geometry, determine the requirements on the jammer. Table I gives the problem geometry (for two cases of terrain roughness) for a possible Terrain Bounce situation.

Choice of β_o

The values chosen for β_o correspond with gently rolling terrain ($\beta_o = .1$ rad), and with very rugged terrain ($\beta_o = 1$ rad). Using the definition (Reference 7: 251):

$$\mathrm{Tan}\,\beta_o = 2\ \sigma_h/T \tag{40}$$

Tan β_o may be interpreted as a mean value of the ratio of vertical to horizontal irregularities, and represents a mean-square value of the slope of the irregularities (Reference 7: 251). For relatively level terrain, if it is assumed that:

$$\sigma_h \sim O(1\ m)$$
$$T \sim O(10\ m)$$

(where $O()$ indicates order of magnitude), then β_o is on the order of .1 rad. For very rough terrain, if it is assumed that:

$$\sigma_h \sim O(1\ m)$$
$$T \sim O(1\ m)$$

then β_o is on the order of 1 rad.

These values for β_o are comparable to the values of β_{max}, (Tan β_{max} = maximum slope of the surface irregularities), where β_{max} is equal to a few degrees ($O(.1$ rad)) for relatively level terrain, and β_{max} approaches $90°$ ($O(1$ rad)) for very rugged terrain.

TABLE I
PROBLEM GEOMETRY

Target Altitude (H_t)	100 m
Target Velocity (v_a)	200 m/sec
Missile Velocity (v_m)	600 - 800 m/sec
Terrain Roughness Factor (β_o)	.1 rad, 1 rad
Range of Expected Dive Angles (θ_a from Missile to Target) Direction of Approach	$5^o - 35^o$ Forward Hemisphere
Transmit Wavelength (λ)	.03 m

The value of β_o for actual terrain may be determined by approximating $\beta_o = \beta_{max}$, and using:

$$\sigma^o = \cot^2 \beta_{max}$$
$$\beta_{max} = \text{Tan}^{-1}(1/\sqrt{\sigma^o}) \tag{41}$$

where σ^o is the measured bistatic scattering coefficient. Note that care should be taken to measure σ^o over a small area of terrain, since averaging its value over an area larger than the glistening area $(|\beta| \leq \beta_{max})$ will result in a reduction in the measured value of σ^o.

Some measurements of σ^o have been published by Ohio State University (Reference 12). The Ohio State data measured the bistatic scattering coefficient for very level terrain. The reflected signals from some terrain samples exhibited very large specular components, indicating that the terrain was not very rough. The data gives β_{max} (averaged over $\psi_r = \psi_t \pm 10^o$) on the order of +15 dB for some terrain samples (loam at $\psi_t = 40^o$, Horizontal Polarization; smooth sand at 40°-70°, Horizontal Polarization), which gives β_{max} on the order of .1 rad. For rougher terrain samples, the reflected signal exhibited very small specular components. The data gives σ^o on the order of -5 dB for some terrain samples (rough sand at $\psi_t = 20^o$, Horizontal Polarization; dry grass at $\psi_t = 20^o$, Horizontal Polarization), which gives β_{max} on the order of 1 rad. Equation (18) for σ^o requires β_{max} to be small enough such that $\beta \approx \text{Tan } \beta$ for $|\beta| \leq \beta_{max}$. This assumption is satisfied only to the order of magnitude for $\beta_{max} = 1$ rad, since $\text{Tan}(1 \text{ rad}) = 1.56$. Thus, the results obtained for $\beta_o = 1$ rad are probably at the limit of the applicability of Equation (18).

Application of Methodology

Limits on θ_{ma}. The limiting cases for the problem geometry of

Table I are given by Equation (39):

$$4^\circ < \theta_{ma} < 28^\circ , \quad \psi = \theta_{ma} \qquad\qquad \text{head-on approach}$$

$$5^\circ < \theta_{ma} < 34^\circ , \quad \psi = \begin{cases} 72^\circ \text{ for } v_m = 600 \text{ m/sec} \\ 76^\circ \text{ for } v_m = 800 \text{ m/sec} \end{cases} \qquad \text{side-on approach}$$

Characteristics of Glistening Area. For the case of $\beta_o = 1$ rad, the glistening area covers much of the range between the target and the receiver. Figure 16 shows the glistening area for a ground range of R=1000 m and $\theta_{ma} = 4^\circ$. Using Equation (26), it is found that ρ_d^2 has a large value in a region roughly 50-150 meters from the base of the target As θ_{ma} and R are varied, the glistening area varies somewhat; but a large value of ρ_d^2 continues to come from a region 50-150 meters from the target. Much of the reflection can be utilized if the jammer antenna illumination is restricted to this area. Using Figure 17, it is found that a jammer antenna depression angle of 50° from the horizontal, and a beamwidth of 30° will illuminate the patch desired. (Note that the size of the glistening area has been substantially reduced by assuming a directive, rather than omnidirectional target antenna pattern.)

For the case of $\beta_o = .1$ rad, the glistening area exhibits quite different behavior than for $\beta_o = 1$ rad. As shown in Figure 18, the position of the glistening area with respect to the target changes with R. It also varies with θ_{ma}. For these reasons, it is not possible to immediately select a jammer antenna pattern which will always illuminate the area desired.

Critical Range. The critical range R_c is calculated using Equation (30). For the case of $\beta_o = 1$ rad, the antenna directivity has already been determined. Thus, R_c is calculated based upon the reduced-sized glistening area, for the desired range of θ_{ma} values. The calculated

46
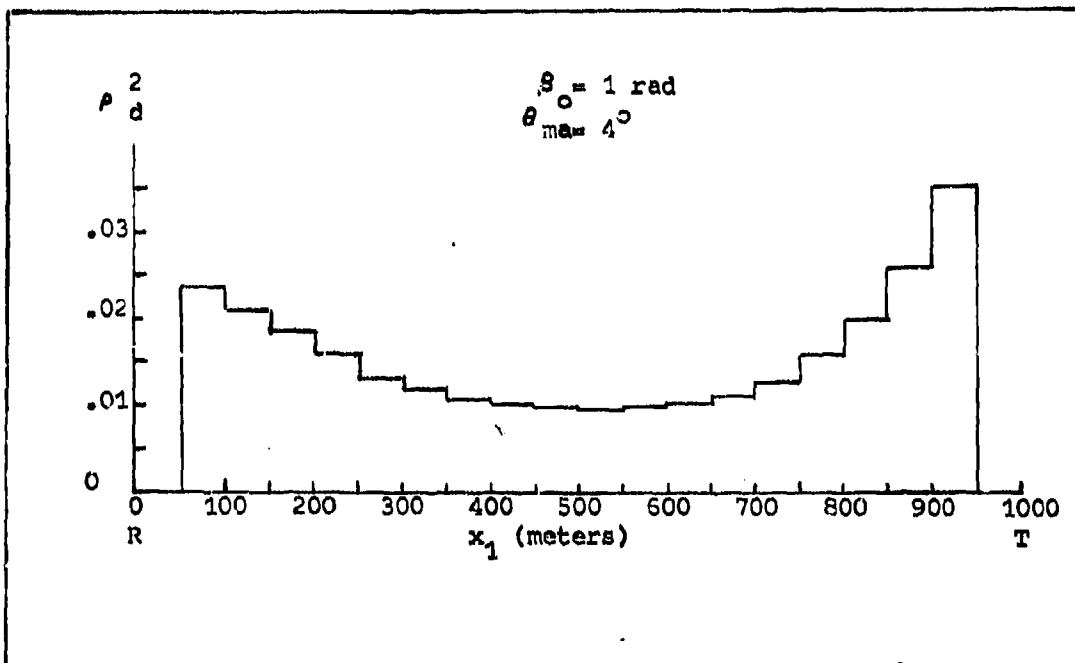
Figure 16. Characteristics of Glistening Area for $\beta_0 = 1$ rad, R= 1000 m, $\theta_{ma} = 4°$
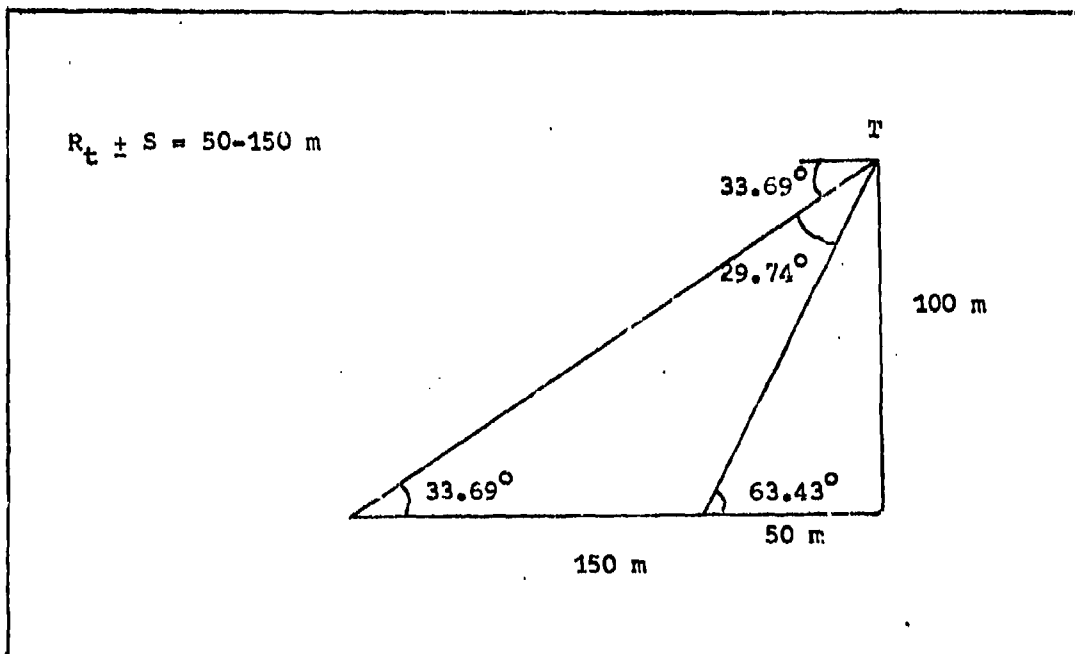
Figure 17. Illumination of Ground Patch for $\beta_0 = 1$ rad

47
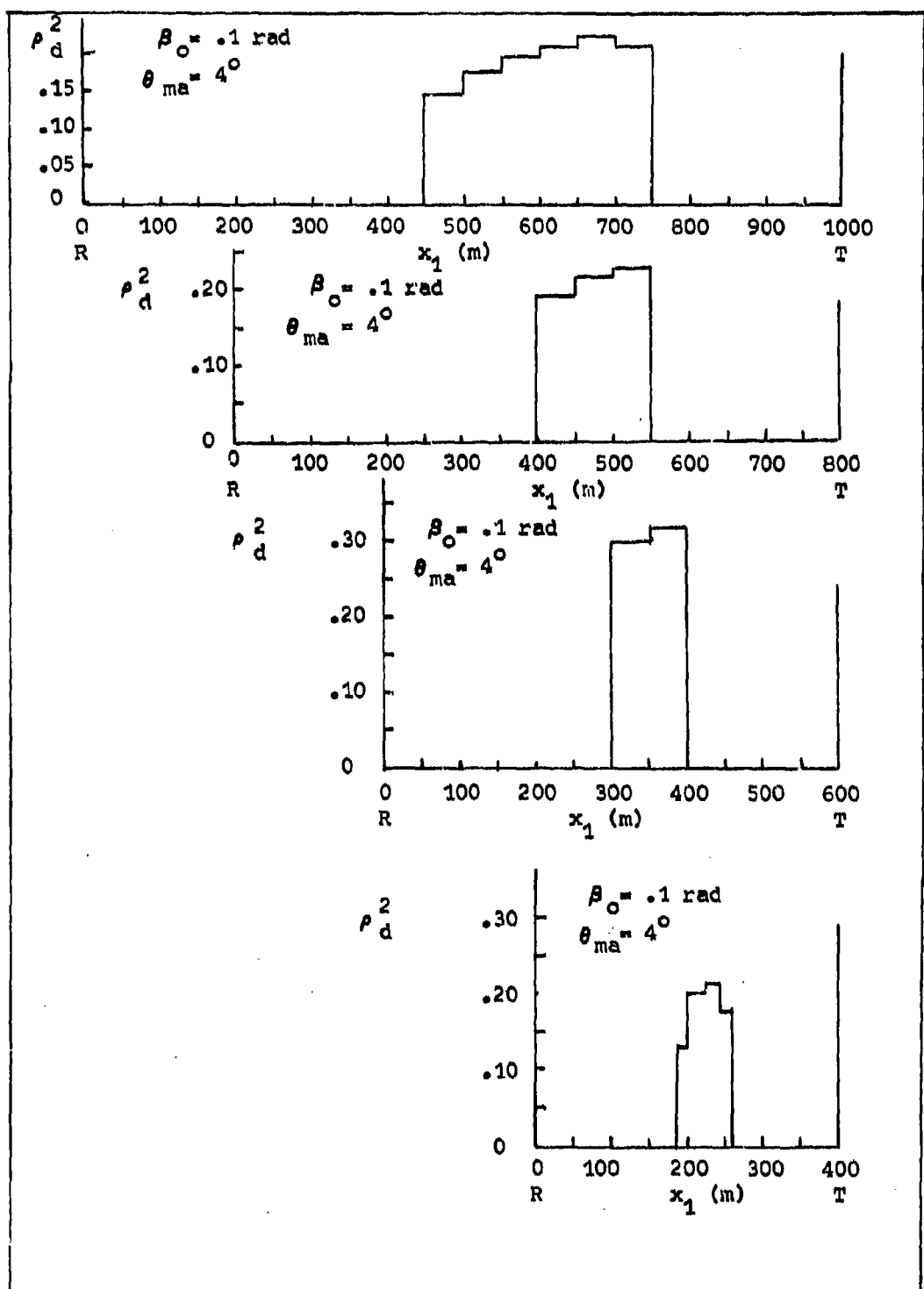
Figure 18. Characteristics of Glistening Area for $\beta_o = .1$ rad, Varying Range, $\theta_{ma} = 4^o$

48

values of R_c are presented in Table II.

For the case of $\beta_o = .1$ rad, R_c is calculated based upon the entire glistening area (unreduced by directive antenna patterns), using the criterion of Equation (37). Figure 19 plots the size and magnitude of the glistening areas for several limiting values of θ_{ma} ($\theta_{ma} = 4^o$ and 28° for head-on approach, and $\theta_{ma} = 5^o$ and 34° for side-on approach). Intermediate values of θ_{ma} generate glistening areas which fall within these limits. From Figure 19, the maximum area to be illuminated extends from 70-510 meters from the target. The calculated values of R_c are presented in Table III.

Size and Magnitude of Glistening Area. Using Equations (25) and (26), the diffuse reflection coefficient (ρ_d^2) may be determined for each case of θ_{ma}, R_c, and ψ. Tables II and III give the calculated values of ρ_d^2 for these two examples. The Tables also include the size and position of each glistening area, using the following parameters:

R_t = ground distance from target to center of glistening area

S = spatial spread of ground patch about the center

The quantity $R_t \pm S/2$ indicates the ground distance of the near and far edges of the ground patch from the target.

Assumption of Point Source at Ground Patch. In calculations up to this point, it has been assumed that the glistening area may be considered as a point target. This assumption may now be validated by comparing the the angular size of the ground patches to the missile 3-dB beamwidth. Since the glistening area is rather narrow in azimuth, the size of the patch in elevation angle is of primary concern. The angular size of the

49

TABLE II

CHARACTERISTICS OF REFLECTED SIGNAL

Geometry of Table I ; $\beta_o = 1$ rad

Approach	θ_{ma}	R_c (m)	$R_t \pm S$ (m)	ρ_d^2	ΔF_1 (Hz) $\begin{cases} v_m = 600 \text{ m/sec} \\ v_m = 800 \text{ m/sec} \end{cases}$
Head-on	$4°$	560	60-140	.05711	1734.4-3533.8
					1942.6-3669.2
	$10°$	580	60-140	.05979	1500.2-3294.0
					1718.6-3422.6
	$15°$	590	60-140	.06193	1237.6-3045.5
					1460.6-3167.6
	$20°$	580	60-140	.06424	940.8-2762.1
					1177.2-2882.8
	$25°$	570	60-140	.06642	579.8-2432.8
					820.7-2548.6
	$28°$	560	60-140	.06776	341.6-2217.1
					584.6-2329.9
Side-on	$5°$	560	60-140	.05768	939.0-1347.2
					1087.7-1072.6-1279.6
	$20°$	580	60-140	.06424	747.8-1132.4
					974.1- 925.6-1085.1
	$34°$	560	60-140	.07065	305.1- 818.7
					598.5- 566.6- 798.4

$\Delta F_t = 305.1 - 3669.2 = 3364.1$ Hz

$(\Delta F_1)_{min} = 160$ Hz

(a) Head-on Approach

(b) Side-on Approach
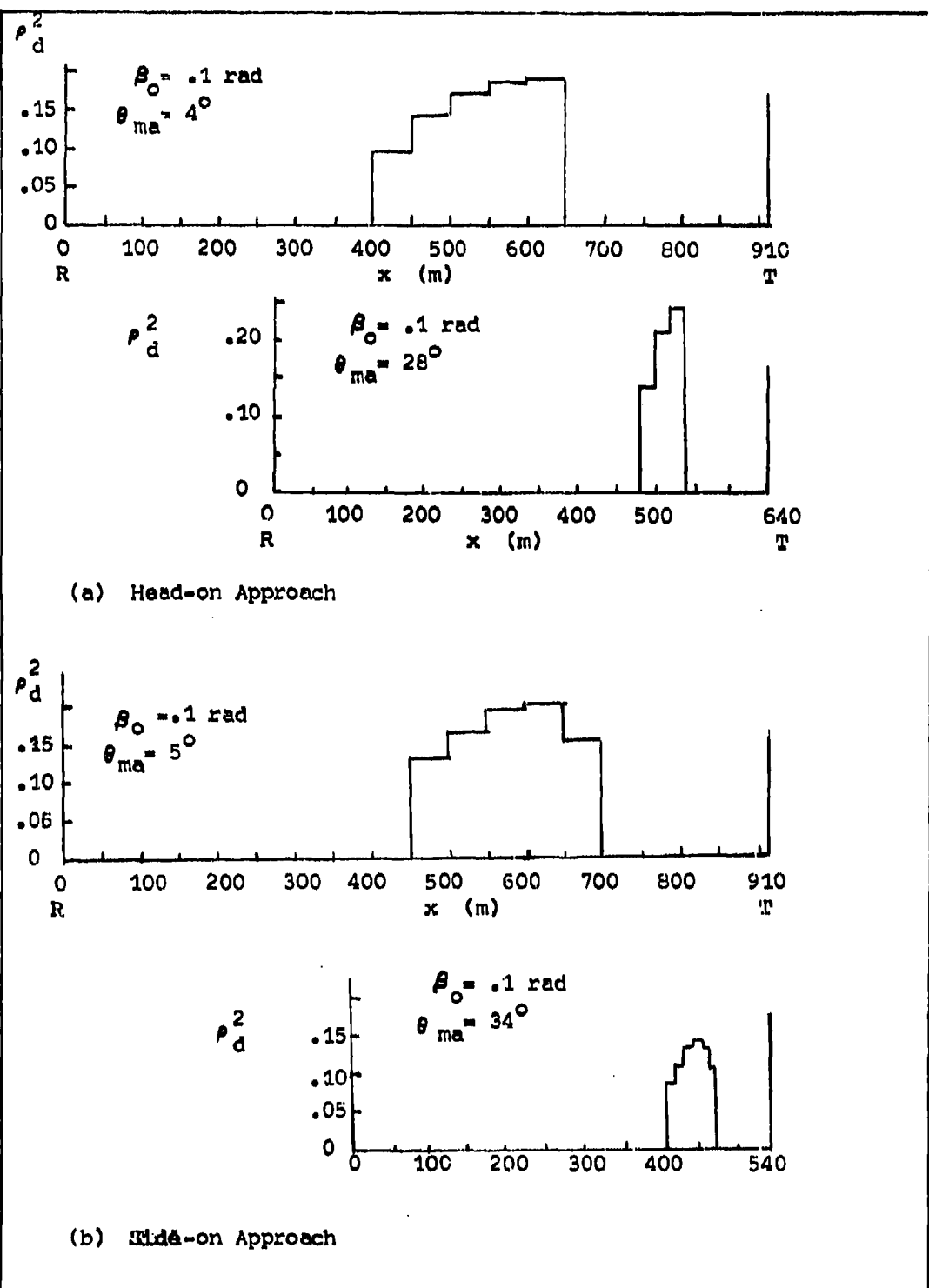
Figure 19. Characteristics of Glistening Area for $\beta_o = .1$ rad, $R = R_c$

51

TABLE III

CHARACTERISTICS OF REFLECTED SIGNAL

Geometry of Table I : $\beta_o = .1$ rad

Approach	θ_{ma}	R_c (m)	$R_t \pm S$ (m)	ρ_d^2	ΔF_1 (Hz) $\begin{cases} v_m = 600 \text{ m/sec} \\ v_m = 800 \text{ m/sec} \end{cases}$
Head-on	4°	910	260-510	.7822	970.4-601.5-660.0
					1306.4-730.4-764.7
	10°	880	180-330	.7437	558.9-541.6-841.9
					871.0-713.9-944.2
	15°	800	140-260	.7731	462.8-1033.3
					697.1-685.4-1144.8
	20°	760	120-220	.7617	277.5-1060.2
					502.7-1172.0
	25°	6BC	100-180	.7282	153.4-1149.9
					377.4-1267.2
	28°	640	100-160	.6046	18.0-1020.5
					295.3-1068.9
Side-on	5°	910	210-460	.8570	793.0-411.8-417.9
					1088.9-474.9
	20°	760	120-220	.7617	508.8-461.0-555.8
					768.5-600.9-618.8
	34°	540	70-130	.6788	349.8-705.1
					627.3-607.9-741.7

$\Delta F_t = 18.0 - 1306.4 \text{ Hz} = 1288.4 \text{ Hz}$

$(\Delta F_1)_{min} = 95 \text{ Hz}$

ground patch is given by:

$$\theta_{size} = \psi_{r,max} - \psi_{r,min} \qquad (42)$$

where $\psi_{r,max}$ occurs at the edge of the ground patch nearest the receiver, and $\psi_{r,min}$ occurs at the edge of the patch nearest the target. From Figure 20:

$$\psi_{r,max} = Tan^{-1}(H_r/(R-x_a))$$
$$\psi_{r,min} = Tan^{-1}(H_t/(R-x_b))$$
$$H_r = H_t + R \, Tan \, \theta_{ma}$$

For the two cases considered here, the maximum θ_{size} is about 8°. This angular size corresponds to less than half the missile beamwidth (θ_{3m}) and the glistening area would appear to be reasonably approximated as a point target.

Doppler Offset and Spreading. Now that the size and location of the glistening area (as modified by the jammer antenna directivity) have been determined (as a function of R_c, θ_{ma}, and ψ), the problems of Doppler offset and spreading may now be addressed. Using Equation (8), the difference in Doppler frequency between the direct path jamming signal and the reflected signal may be calculated for points along the glistening area at intervals Δx. The reflected signal associated with each point must be spread in Doppler to account for the uncertainty in v_m (i.e., 600 m/sec $< v_m <$ 800 m/sec in Equation (8)). From one end of the glistening area to the other, the range of Doppler offsets (ΔF_1) is determined. Tables II and III list ΔF_1 for the two cases considered here. Due to uncertainty in the problem geometry, the ranges of ΔF_1 which arise from all possible values of R_c, θ_{ma}, and ψ must be covered by the jammer.

53
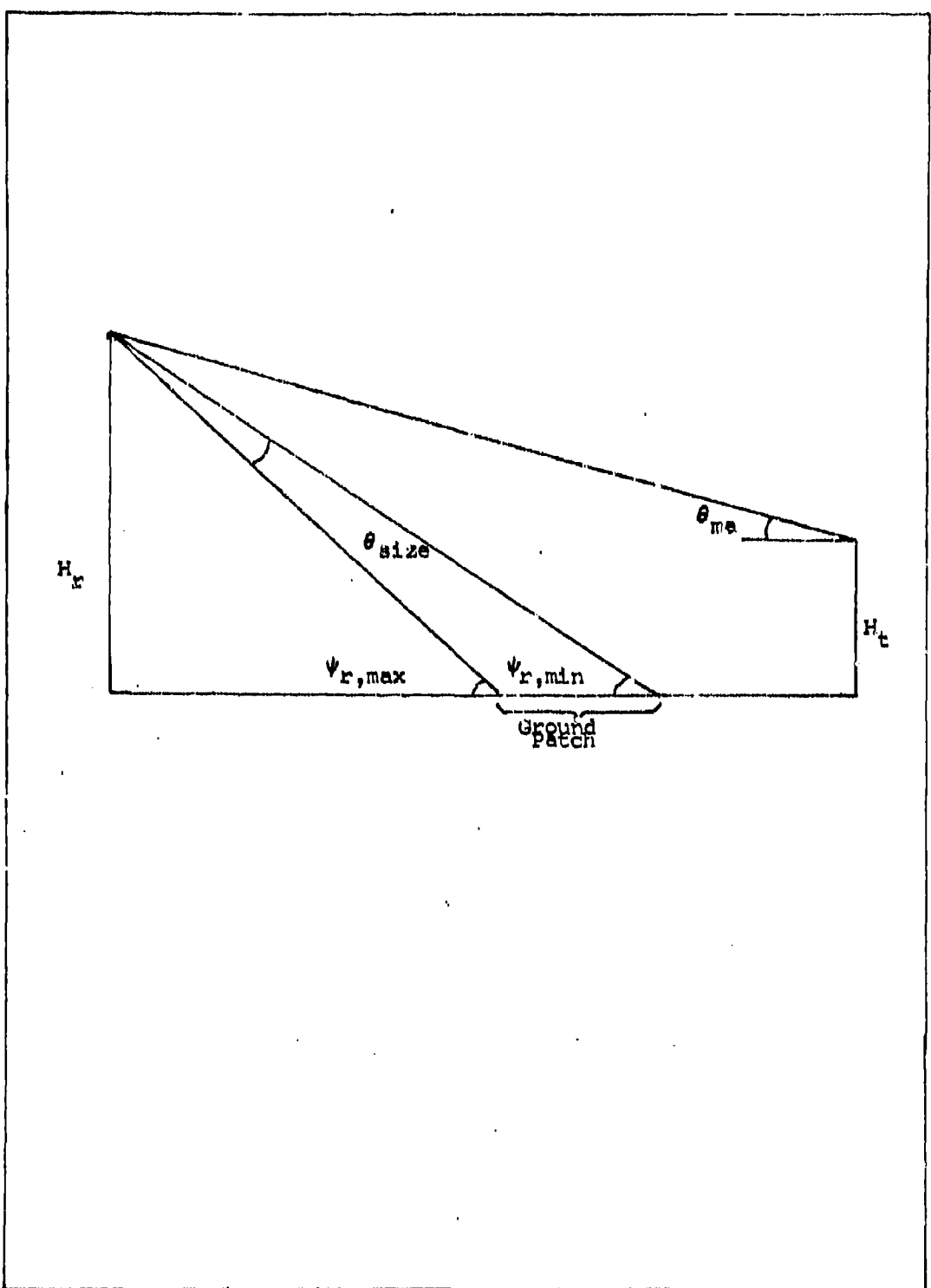
Figure 20. Angular Size of Ground Patch

This total range (ΔF_t) is given for each case of θ_{ma} in Tables IV and V. The additional spreading which is described by Equation (27) is also included in Tables IV and V. In both cases, F_g is substantially smaller than ΔF_t, and will be neglected.

Jammer Requirements

Jammer Antenna Orientation. The jammer antenna orientation may be established based upon the location of the ground patch that is required to be illuminated. For $\beta_o = 1$ rad, the antenna orientation has already been assumed ($\theta_{depr} = 50^\circ$, $\theta_{3a} = 30^\circ$). For $\beta_o = .1$ rad, the area to be illuminated extends from 70-510 meters from the target. From Figure 21, it may be concluded that an antenna depression angle of 33° and a 3-dB beamwidth of 44° would illuminate the entire ground patch desired.

Thus, the antenna directivity in elevation has been established. However, the illumination of the terrain in azimuth is also of concern. Using Equation (17) for y (the width of the glistening area), it is found that for either case ($\beta_o = 1$ rad, or $\beta_o = .1$ rad), the glistening area is rather narrow in azimuth. Thus, an area almost directly between the receiver (missile) and the target (aircraft) must be illuminated at all times. Since the angle of approach of the missile is unknown within the forward hemisphere, it is necessary to illuminate half of an annular region around the aircraft. (See Figure 22.)

Doppler Offset and Additional Spreading. Using Equations (11) and (12), the required jammer Doppler offset (f_{jo}) and spreading (ΔF_s) may be calculated. However, it may be seen that for both cases, f_{min} does not satisfy Equation (13). Thus, Equations (14) and (15) are used for both cases (using $f' = 600$ Hz). The calculated values of f'_{jo}, $\Delta F'_s$, and ΔF_j are given in Tables IV and V.

Diffuse Reflection Coefficient. Using Equation (26) one may find

56

TABLE IV

SUMMARY OF CHARACTERISTICS OF REFLECTED SIGNAL

$$\beta_o = 1 \text{ rad}$$

Characteristics of Reflected Signal		Jammer and Antenna Requirements	
$R_t \pm S$	$= 60\text{-}140$ m	$\theta_{depr} = 50^\circ$	
		$\theta_{3a} = 30^\circ$	
ΔF_t	$= 2364.1$ Hz	$f_{jo} = 1987$ Hz	$f'_{jo} = 2150$ Hz
F_g	$= 155.7$ Hz	$\Delta F_s = 4364$ Hz	$\Delta F'_s = 3300$ Hz
		$(\pm 2182$ Hz$)$	$(\pm 1650$ Hz$)$
	''	$\Delta F_j = \Delta F'_s - (\Delta F_i)_{min}$	
		$3300 - 160 = 3140$ Hz	
ρ^2_d	$= .05711$ *		

---

* Does not account for losses due to absorption by terrain.

TABLE V

SUMMARY OF CHARACTERISTICS OF REFLECTED SIGNAL

$$\beta_o = .1 \text{ rad}$$

Characteristics of Reflected Signal		Jammer and Antenna Requirements			
$R_t \pm S$	$= 70\text{-}510$ m	$\theta_{depr} = 33^o$ $\theta_{3a} = 44^o$			
ΔF_t	$= 1288.4$ Hz	$f_{jo} = 662$ Hz		$f'_{jo} = 950$ Hz	
F_g	$= 10.0$ Hz	$\Delta F_s = 2288$ Hz (± 1144 Hz)		$\Delta F'_s = 900$ Hz (± 450 Hz)	
		$\Delta F_j = \Delta F'_s - (\Delta F_i)_{min}$ $= 900 - 95 = 805$ Hz			
ρ_d^2	$= .6046$ *				

* Does not account for losses due to absorption by terrain.
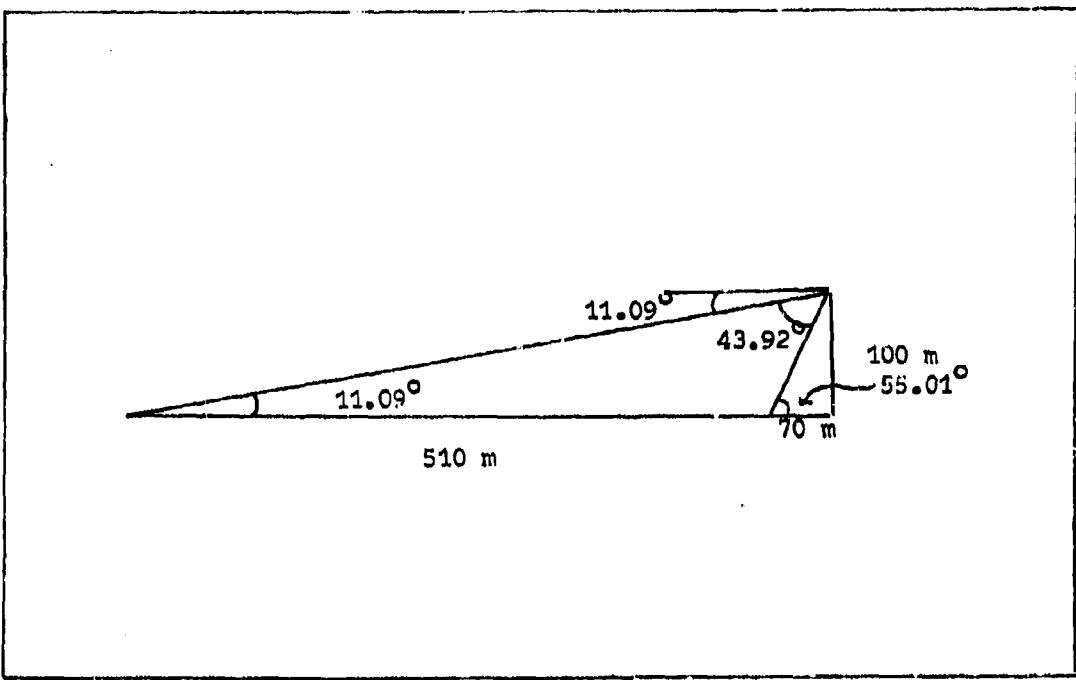
Figure 21. Illumination of Ground Patch for β_o = .1 rad
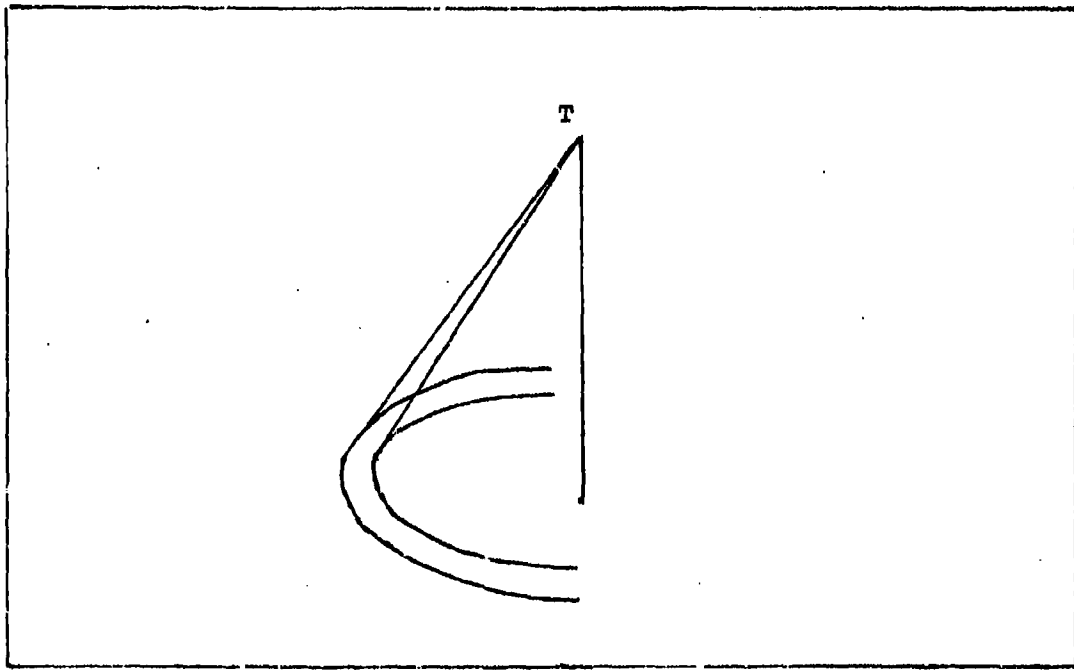
Figure 22. Illumination in Azimuth for Jamming in Forward Hemisphere

the diffuse reflection coefficient ρ_d^2. (Tables II and III give the values of ρ_d^2 for various cases included in the problem being considered.) The reflection coefficient is used in Equation (2) to determine the System J/S and antenna sidelobe levels (G_{jm}/G_{jg}) required of the jammer.

Since the jammer must be adequate for even the worst case of reflection, the minimum value of ρ_d^2 is chosen for use in Equation (2). (See Tables IV and V.) Since ρ_d^2 has been derived from an idealized model, (rather than measured from actual terrain), it must be reduced to account for loss (L_a) due to absorption by the terrain. (Note that the loss factor should not be included here if it has already been incorporated into the terrain model, or if ρ_d^2 is a measured value.) It is assumed that $L_a = 10$, which is a reasonable value (to the order of magnitude) for vegetation-covered terrain (Reference 3; 690). Actual absorption losses are a function of terrain covering (vegetation, soil, etc.), moisture content, and frequency.

Using the calculated value for ρ_d^2; the selected value for $\Delta\theta/\theta_{3m}$ (=.643 from Equation (31)); and assuming a value of $\theta_s/\theta_{3m} = .3$, Equation (2) may be plotted in terms of the angular error $\theta/\Delta\theta$ vs. $(J/S)_s$ for various values of G_t. (See Figures 23 and 24.) From Equation (32), the angular error is required to be .777. The plots show the value of $(J/S)_s$ which is required for a particular value of G_t.

The parameter G_t is given by Equation (4):

$$G_t = (G_{jm}/G_{jg}) \qquad (43)$$

where G_{jm}/G_{jg} determines the required jammer sidelobe level.

Loss Factor. In general, G_t must be reduced by a loss factor (L). The loss factor may be broken up into a loss and a gain factor which
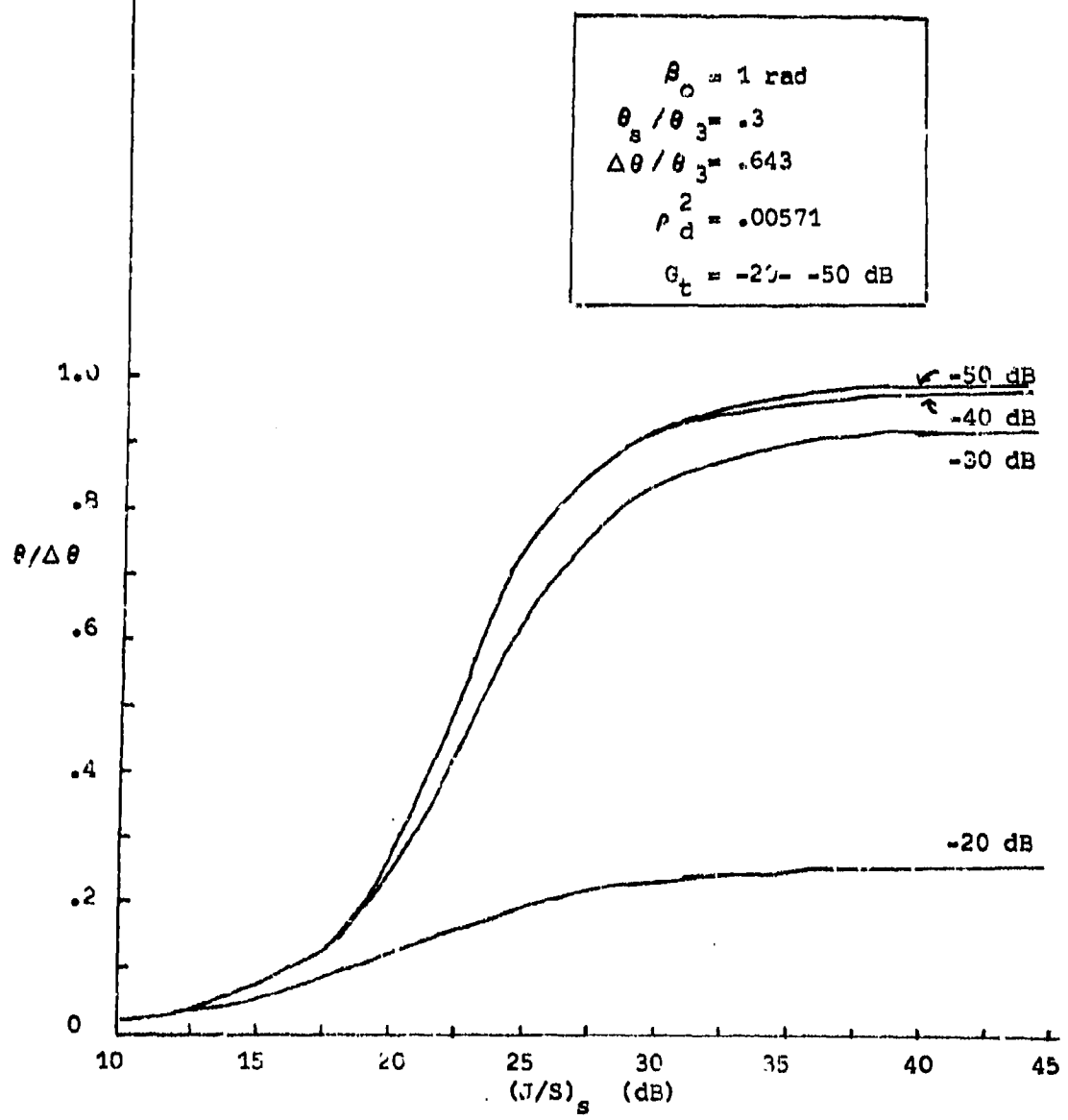
Figure 23. Angular Error vs. System J/S (β_o = 1 rad)

61
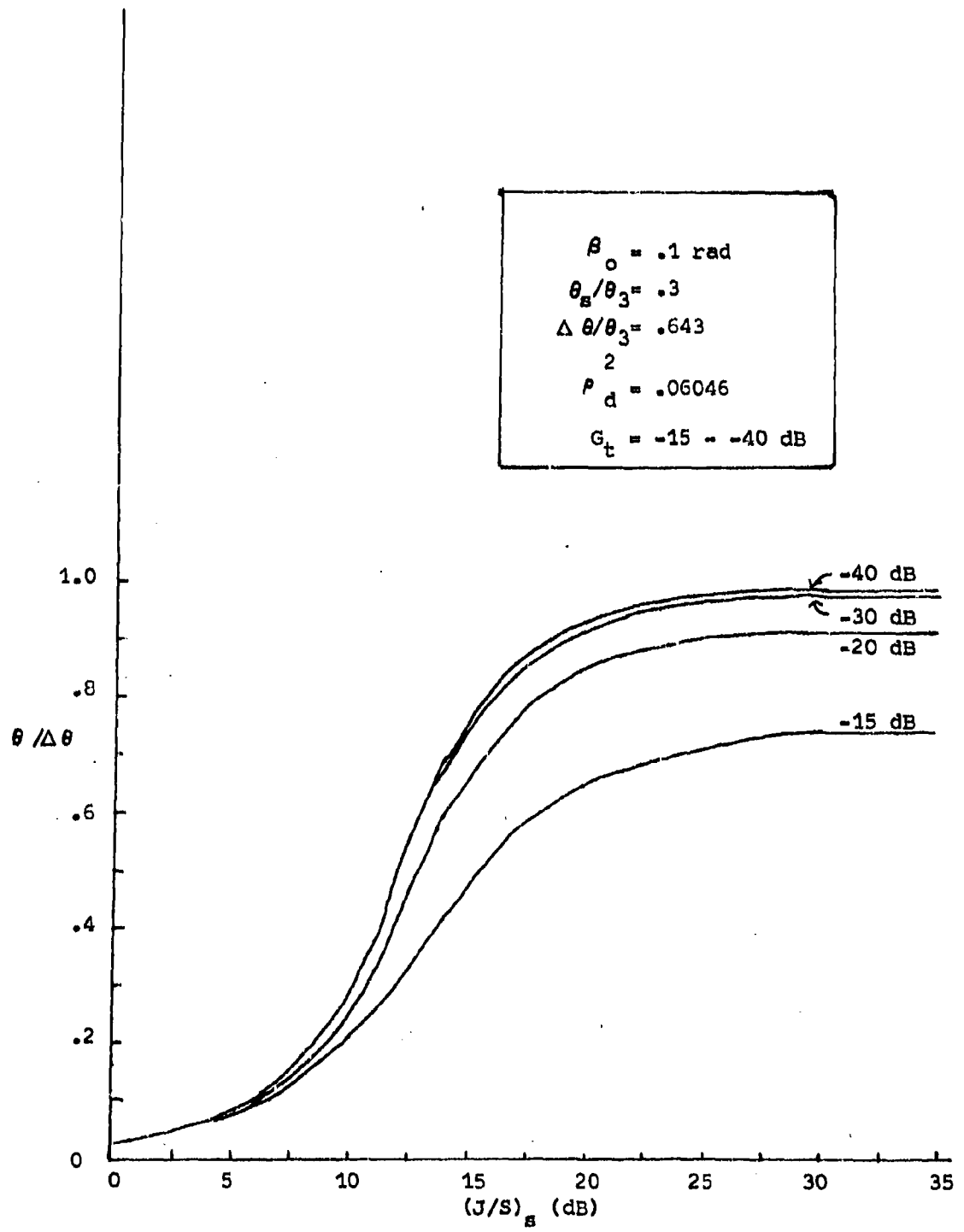
Figure 24. Angular Error vs. System J/S (β_o = .1 rad)

affect the countermeasure:

$$L = F / L_s \qquad (44)$$

where L_s is the loss due to Doppler spreading of the signal, and F is the gain due to shifting of the direct path jamming signal out of the Doppler Bandwidth of the missile.

The loss due to Doppler spreading by the jammer (L_s), is the amount by which the spread jamming signal exceeds the Doppler Bandwidth of the missile.

$$L_s = \Delta F_s / BW \qquad (45)$$

where BW is the missile Doppler Bandwidth in Hz.

A Doppler filter parameter F will be used to represent the gain due to shifting the direct path jamming signal out of the missile's Doppler bandwidth (to an assumed -30 dB Doppler filter sideband level):

$$F = \begin{cases} 0 \text{ dB} & \text{if direct path jamming signal falls within missile Doppler Bandwidth} \\ +30 \text{ dB} & \text{if direct path jamming signal falls outside missile Doppler Bandwidth} \end{cases} \qquad (46)$$

Tables VI and VII give the losses and gains for the two cases considered here, along with G_{jm}/G_{jg}.

System J/S vs. Sidelobe Levels. Using Equation (43) and the calculated loss and gain factors, the required jammer System J/S may be related directly to the antenna sidelobe levels (G_{jm}/G_{jg}). Table VIII summarizes the results for the two cases of the problem under consideration.

Results

For the problem geometry of Table I, (with β_o=1 rad, and β_o=.1 rad),

TABLE VI
SYSTEM J/S AND JAMMER SIDELOBE LEVELS
$$\beta_o = 1 \text{ rad}$$

$$\rho^2_d / L_a = .05711/10 = .005711$$

G_t	G_{jm}/G_{jg}	$(J/S)_s$
-50 dB	-26.02 dB	25.5 dB
-40 dB	-16.02 dB	25.5 dB
-30 dB	- 6.02 dB	27.5 dB

$G_t = (G_{jm}/G_{jg})/(F/L_s)$
$L_s = -6.02$ dB $\qquad\qquad$ F $= +30$ dB
G_t dB + 23.98 dB $= G_{jm}/G_{jg}$ dB

TABLE VII
SYSTEM J/S AND JAMMER SIDELOBE LEVELS
$$\beta_o = .1 \text{ rad}$$

$$\rho^2_d / L_a = .6046/10 = .06046$$

G_t	G_{jm}/G_{jg}	$(J/S)_s$
-50 dB	-22.30 dB	15.3 dB
-40 dB	-12.30 dB	15.3 dB
-30 dB	- 2.30 dB	15.5 dB

$G_t = (G_{jm}/G_{jg})/(F/L_s)$
$L_s = -2.30$ dB $\qquad\qquad$ F $= + 30$ dB
G_t dB + 27.70 dB $= G_{jm}/G_{jg}$ dB

TABLE VIII

SUMMARY OF JAMMER REQUIREMENTS FOR PROBLEM GEOMETRY OF TABLE I

	$\beta_o = 1$ rad	$\beta_o = .1$ rad
Beamwidth (θ_{3a})	50°	33°
Depression Angle (θ_{depr})	30°	44°
Doppler Offset (f'_{jo})	2150 Hz	950 Hz
Doppler Spread ($\Delta F'_s$)	3300 Hz	900 Hz
	(± 1650 Hz)	(± 450 Hz)
Additional Spread (ΔF_j)	3140 Hz	805 Hz
Azimuth Coverage	180°	180°
$\Delta\theta / \theta_{3m}$	.643	.643
$\theta / \Delta\theta$	.777	.777

G_{jm}/G_{jg}	$(J/S)_s$	G_{jm}/G_{jg}	$(J/S)_s$
-26.02 dB	25.5 dB	- 22.30 dB	15.3 dB
-16.02 dB	25.5 dB	- 12.30 dB	15.3 dB
- 6.02 dB	27.5 dB	- 2.30 dB	15.5 dB

the jammer antenna directivity (depression angle, elevation and azimuth beamwidths), sidelobe levels (G_{jm}/G_{jg}) have been determined, along with the required Doppler offset (f_{jo}) and additional spreading (ΔF_j) and $(J/S)_s$ for the jammer. These results are summarized in Table VIII. The Doppler offset and spreading permit most of the illuminated terrain to reflect at frequencies which will fall within the missile's Doppler Bandwidth. At the same time, the jammer's direct path signal is shifted outside the Doppler Bandwidth, (greatly reducing the required jammer sidelobe levels for a given $(J/S)_s$).

In general, the jammer requirements of Table VIII should be attainable with state-of-the-art technology. Note that for G_t greater than some maximum, the required angular error can not be achieved for any System J/S. For G_t below some level (about -40 dB for either case of β_o), a further reduction in G_t does not substantially reduce $(J/S)_s$.

Problems for Jammer

Approach From Rear Hemisphere. The geometry not treated in the preceeding example is that for missile approach from the rear hemisphere. Preliminary investigation of approach from this direction indicates that the Terrain Bounce Countermeasure will not be as successful for this geometry, as it may be for forward approach. (See Tables IX and X.) The ground-bounced signal may have zero Doppler offset from the direct path signal. This phenomena would require the jammer to do one of the following:

1. Utilize only a small fraction of the possible reflected signal offsets. (This will substantially lower the reflection coefficient ρ_d^2, and thereby require higher System J/S and lower jammer antenna sidelobe levels.)

TABLE IX

TAIL-ON APPROACH

Geometry of Table I : $\beta_o = 1$ rad

Approach	θ_{ma}	R_c (m)	$R_t \pm S$ (m)	ρ_d^2	ΔF_1 (Hz) $v_m = 600$ m/sec	ΔF_1 (Hz) $v_m = 800$ m/sec
Tail-on	7°	580	60-140	.05822	− 377.0--2646.9	− 171.7--2520.0
	10°	580	60-140	.05979	− 195.1--2525.7	+ 22.8--2397.5
	20°	580	60-140	.06424	+ 460.8--2046.0	+ 696.9--1925.4
	30°	550	60-140	.06868	+1020.5--1929.4	+1244.9--1829.8
	40°	480	60-140	.07359	+2243.7-- 619.5	+2504.3-- 513.9
	50°	390	60-140	.07971	+3027.4-- 273.8	+3269.1-- 190.6

$\Delta F_t = +3269.1--2646.9 = 5916.0$ Hz

TABLE X

TAIL-ON APPROACH

Geometry of Table I : $\beta_o = .1$ rad
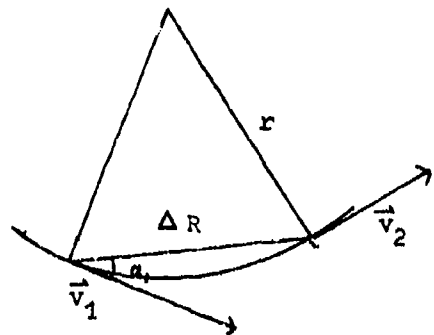
Approach	θ_{ma}	R_c (m)	$R_t \pm S$ (m)	ρ_d^2	ΔF_1 (Hz) $v_m = 600$ m/sec	ΔF_1 (Hz) $v_m = 800$ m/sec
Tail-on	7°	910	210-410	.7891	+ 851.2--167.0	+1107.7-- 69.4
	10°	880	180-330	.7434	+ 781.6--231.8	+1005.4--130.1
	20°	760	120-220	.7617	+1057.4--397.8	+1282.4--286.3
	30°	600	80-140	.6619	+1062.8--653.9	+1266.9--538.0
	40°	430	60-100	.5396	+1284.8--467.5	+1497.7--337.4
	50°	290	40- 70	.4366	+1301.0--524.0	+1496.1--405.1

$\Delta F_t = +1497.7--653.9 = 2151.6$ Hz

2. Utilize all possible reflected signal offsets. (This will allow
the spread jammer direct path signal to remain within the missile's
Doppler Bandwidth. Consequently, the gain factor F (from Equation (46)
becomes 0 dB, and significantly lower antenna sidelobe levels will be
required for a given $(J/S)_s$.)
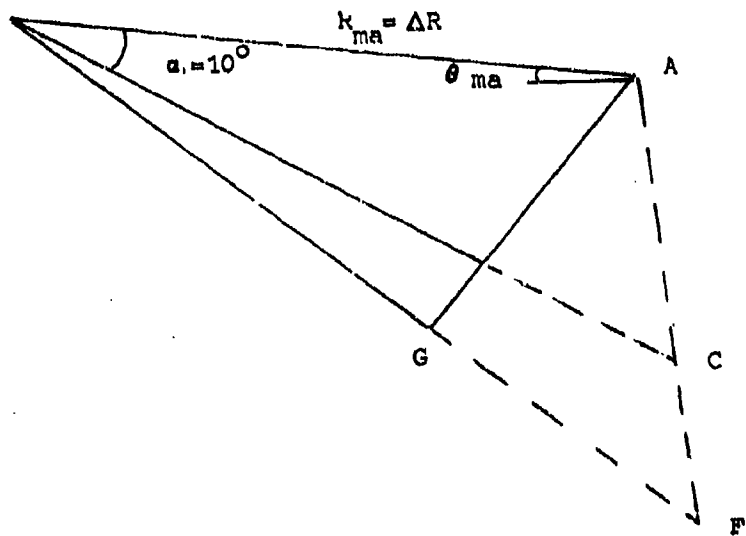
Disappearance of Ground Target. A fundamental problem with the
Terrain Bounce Countermeasure is that it may be disrupted by large dis-
continuities in the terrain. The terrain model developed in Section II
involves reflection from many elementary facets of the terrain. This
permits the assumption that any fluctuations in the reflected signal
(due to changing R and θ_{ma}) will be rapid and (on the average) have no
effect on the tracking. However, if the terrain exhibits large discon-
tinuities (for example, buildings or cliffs), it is possible that the
ground patch may disappear entirely from the missile beam. If the ground
target disappears at a range greater than R_c then there is a good chance
that it will reappear before the missile deviates from its course enough
to matter, (provided that the discontinuity is very short in extent).
If the ground target disappears at a range less than R_c, then there is
little chance that the missile can reacquire the true target (since
the target is already outside the missile's 3-dB beamwidth). Thus, we
are primarily concerned about the disappearance of the ground target at
the critical range R_c.

It is assumed that the missile is tracking the power centroid at
range R_c. If the ground target disappears at this time (causing the
power centroid to shift up to the aircraft), the missile will change
course in an attempt to impact the aircraft.

Figure 25 shows the geometry of the problem. $\vec{v}_1$ is the initial

68

(a) Change of velocity vector from $\vec{v}_1$ (aimed at impact with power centroid) to $\vec{v}_2$ (aimed at impact with true target)

(b) Angular separation of target and power centroid

Figure 25. Normal Acceleration of Missile

velocity vector of the missile, aimed at the projected point of impact with the power centroid. $\vec{v}_2$ is the corrected velocity vector, (that necessary in order to impact with the actual target). If the power centroid should disappear at the critical range R_c, the missile will undergo an acceleration to correct its velocity vector to $\vec{v}_2$. It is assumed that the missile undergoes normal acceleration, (that is, the magnitude of its velocity vector does not change). The normal acceleration (a) required for a direct hit is given by:

$$a = v_m^2 /r \tag{47}$$

where $r = \Delta R/(2 \sin a_1)$, from Figure 25, v_m is the magnitude of $\vec{v}_1$ and $\vec{v}_2$. a_1 is given by Equation (28) ($a_1 = 10^\circ$). And $\Delta R = R_{ma} = R/\cos \theta_{ma}$. Thus the required acceleration is given by:

$$a = 2 \sin(10^\circ) \, v_m \cos \theta_{ma}/R_c = .3472 \, v_m \cos \theta_{ma}/R_c \tag{48}$$

Assuming that the missile has a radius of kill of 20 meters, R_c in Equation (48) is replaced by $R_c \pm 20$ m. Calculations of Equation (48) for the extreme values of θ_{ma} are given in Table XI. For a missile with a maximum acceleration capability of 20 g's, (approximately 200 m/sec), the calculations indicate that a miss can not be guaranteed for the problem geometry of Table I. For $v_m = 800$ m/sec there will be a miss for all target geometries considered. However, for $v_m = 600$ m/sec, there may be a hit for almost all target geometries, and the countermeasure may be unsuccessful. (Note, however, that the missile may still be driven off target if the ground patch reappears within the missile beamwidth.)

Thus, if the reflecting ground patch disappears at the critical range R_c, the success of the countermeasure is questionanle. Although v_m and θ_{ma} can not be controlled by the target aircraft, the aircraft

TABLE XI

MISSILE ACCELERATION REQUIRED FOR TARGET HIT
Missile Kill Radius = 20 m

$$\beta_o = 1 \text{ rad}$$

Approach	R_c (m)	θ_{ma}	a (m/sec^2) (v_m=600 m/sec)	a (m/sec^2) (v_m=800 m/sec)
Head-on	560	4°	215.0-231.0	382.3-410.6
	560	28°	190.3-204.4	338.4-363.4
Side-on	560	5°	214.7-230.6	381.8-410.0
	560	34°	178.7-192.0	317.7-341.3
Tail-on	580	7°	206.8-221.6	367.7-394.0
	390	50°	196.0-217.2	348.5-386.2

$$\beta_o = .1 \text{ rad}$$

Approach	R_c (m)	θ_{ma}	a (m/sec^2) (v_m=600 m/sec)	a (m/sec^2) (v_m=800 m/sec)
Head-on	910	4°	134.1-140.1	238.4-249.1
	640	28°	167.3-178.1	297.4-316.5
Side-on	910	5°	133.9-139.9	238.1-248.8
	540	34°	185.1-199.3	329.1-354.4
Tail-on	910	7°	133.4-139.4	237.2-247.9
	290	50°	259.3-297.7	460.9-529.2

altitude (which establishes the location of the glistening area, and consequently R_c), can be controlled. For the specific missile capabilities expected to be encountered, it may possible to tailor the problem for the desired target miss.

IV. Summary, Conclusions, and Recommendations

Summary

In Section II, the theoretical basis for the Terrain Bounce Countermeasure was developed. This included analysis of the two-target tracking problem, the Doppler offset of the terrain-reflected signal, and a model for rough terrain. A methodology was presented for solving the Terrain Bounce problem. In Section III, the methodology was applied to a specific problem geometry (Table I). The resulting jammer requirements are given in Table VIII.

Conclusions

On the basis of this research, it may be concluded that the jammer requirements for the Terrain Bounce Countermeasure (for missile approach from the forward hemisphere) appear to be achievable within the state-of-the-art of antenna design, for the particular problem geometry and missile IF Bandwidth assumptions used in the calculations. Doppler offset and spreading of the jamming signal permit most of the illuminated terrain to reflect at frequencies which will fall within the missile Doppler Bandwidth. At the same time, the jammer's direct path signal may be shifted outside the Doppler Bandwidth (greatly reducing the required jammer sidelobe levels for a given System J/S). The jammer requirements for an actual Terrain Bounce problem are dependent upon the problem geometry, the uncertainties in that geometry, certain missile parameters (IF Bandwidth and antenna pattern), and the terrain reflectivity.

For jammer antenna sidelobe levels greater than some maximum value, the required angular error can not be achieved for any System J/S. For sidelobe levels below some level, any further reduction in the sidelobe level does not substantially reduce the required System J/S.

A preliminary study of the Terrain Bounce problem for missile

approach from the rear hemisphere indicates that the jammer require-
ments may be much more stringent than those for the forward hemisphere,
since the jammer may not be able to shift the direct path jamming signal
outside the missile Doppler Bandwidth without sacrificing most of the
reflection from the terrain.

The success of the Terrain Bounce Countermeasure is doubtful if
discontinuities in the terrain cause the ground patch target to disappear
at the critical range.

In general, the success of Terrain Bounce Jamming depends upon
illumination of a patch of ground which will reflect adequate energy
towards the missile. This requires knowledge of the roughness of the
terrain, as well as terrain absorption losses. It was found that the
Doppler shifting required of the jamming signal (in order to force the
reflected signal into the missile's Doppler Bandwidth) may be employed
to shift the direct-path jamming signal out of the Doppler Bandwidth.
This phenomena greatly reduces the requirements for low antenna sidelobe
levels, and should be utilized if at all possible.

Recommendations

It is recommended that the Terrain Bounce problem be examined
further for the case of missile approach from the rear hemisphere.

It is also recommended that quantitative measurements of σ° be
made on terrain types which are likely to be involved in a Terrain-
Bounce situation. Many experiments have been done for monostatic
reflection, but the data available on bistatic reflection is sparse,
and is highly dependent upon measurement technique. In particular, care
should be taken to measure the parameter over small areas, since the
illumination of a ground patch which is larger than the glistening area
will result in an average σ° which is smaller than the theoretical

value.

Further investigation into the effects of fluctuation of the reflected signal at discontinuities in the terrain is also desirable.

Bibliography

1. Ament, W.S. "Forward- and Back-Scattering From Certain Rough Surfaces", IRE Transactions on Antennas and Propagation, AP-4: 369-373 (1956).

2. Ament, W.S. "Toward a Theory of Reflection by a Rough Surface", Proceedings of the IRE, 41: 142-146 (1953).

3. Barton, David K. "Low Angle Radar Tracking", Proceedings of the IEEE, 62: 687-704 (June 74).

4. Beard, C.I. "Coherent and Incoherent Scattering of Microwaves from the Ocean", IRE Transactions on Antennas and Propagation, AP-9: 470-483 (Sept, 1961).

5. Beard, C.I., I. Katz, and L.M. Spetner. "Phenomenological Vector Model of Microwave Reflection from the Ocean", IRE Transactions on Antennas and Propagation, AP-4: 162-167 (1956).

6. Beckmann, Petr. "Scattering by Composite Rough Surfaces", Proceedings of the IEEE, 53: 1012-1015 (Aug 65).

7. Beckmann, Petr and Andre Spizzichino. The Scattering of Electromagnetic Waves from Rough Surfaces. N.Y.: Macmillan Co., 1963.

8. Besserer, C.W. Missile Engineering Handbook. Princeton, N.J.: D. Van Nostrand Co., Inc., 1958.

9. Blake, Lamont V. "Reflection of Radio Waves from a Rough Sea", Proceedings of the IRE, 38: 301-304, (1950).

10. Bullington, Kenneth. "Reflection Coefficients of Irregular Terrain", Proceedings of the IRE, 42: 1258-1262 (1954).

11. Cosgriff, R.L., R.L. Peake, and R.C. Taylor. Terrain Scattering Properties for Sensor System Design (Terrain Handbook II). Columbus: Engineering Experiment Station, College of Engineering, The Ohio State University, May 1960.

12. Cost, Stephen T. Measurements of Bistatic Echo Area of Terrain at X-Band. Report 1822-2, Antenna Laboratory. Columbus: The Ohio State University, 15 May 1965.

13. Davies, H. "The Reflection of Electromagnetic Waves from Rough Surface", Proceedings of the IEE, 101, Pt IV: 209-214, (1954).

14. Dept. of the Air Force. Guided Missiles: Operations, Design, and Theory. N.Y.: McGraw-Hill Book Co., Inc., 1958.

15. Durlach, N.I. Influence of the Earth's Surface on Radar. MIT/Lincoln Lab Technical Report 373, Jan 1965. (AD627635).

16. Kell, Robert E. "On the Derivation of Bistatic RCS from Monostatic Measurements", Proceedings of the IEEE, 53: 983-988, (Aug 65).

17. Kerr, Donald E. Propagation of Short Radio Waves. N.Y.: McGraw-Hill Book Co., Inc. 1951.

18. Locke, Arthur S., et al. Guidance. Princeton, N.J.: D. Van Nostrand Co., Inc., 1955.

19. Long, Maurice W. Radar Reflectivity of Land and Sea. Lexington, Mass.: Lexington Books, D.C. Heath and Co., 1975.

20. Moore, R.K. and B.E. Parkins. "Omnidirectional Scattering of Acoustic Waves from Rough Surfaces of Known Statistics", Journal of the Acoustical Society of America, 50: 170-175 (1966).

21. Rice, Stephen O. "Reflection of Electromagnetic Waves from Slightly Rough Surfaces", Communications on Pure Applied Mathematics, 4: 351-378 (1951).

22. Sherwood, E.M. and E.L. Ginzton. "Reflection Coefficients of Irregular Terrain at 10 cm", Proceedings of the IRE, 43: 877-878, (July 55).

23. Spetner, L.M. "A Statistical Model for Forward Scattering of Waves Off a Rough Surface", IRE Transactions on Antennas and Propagation, AP-6: 88-94 (Jan 58).

24. Spetner, L.M. and I. Katz. "Two Statistical Models for Radar Terrain Return", IRE Transactions on Antennas and Propagation, AP-8: 242-246 (May 60).

25. Twersky, Victor. "On Scattering and Reflection of Electromagnetic Waves by Rough Surfaces", IRE Transactions on Antennas and Propagation, AP-5: 81-90 (1957).

26. Vakin, S.A. and L.N. Shustov. Principles of Jamming and Electronic Reconnaissance. Translation of Osnovy Radioprotivodystviya i Radioteckhnicheskoy Rqzvedki. Izd-vo "Sovetskoye Radio". Moscow: 1968. (AD692642).

27. Van Blaricum, Glen. "Ground Reflection Jamming (U)" Appendix E to Strategic Bomber Study Vol 9: Electronic Countermeasures for the Future Bomber Force (S). GRC-CR-2-772, May 1979.

Appendix A

Derivation of Received Voltage at Phase Detector (v_{pd})

Equations (1) and (2) of Section II are derived in this Appendix. (Reference 26: Chapter 4, 186-189).

For the Amplitude-Comparison Monopulse system and noncoherent sources, the signals at the outputs of the two antennas are:

$$v_1 = V_1 \, g(\theta_1 - \theta_s) \, \cos \omega_1 t + V_2 \, g(\theta_2 - \theta_s) \, \cos \omega_2 t$$

$$v_2 = V_1 \, g(\theta_1 + \theta_s) \, \cos \omega_1 t + V_2 \, g(\theta_2 + \theta_s) \, \cos \omega_2 t$$

where θ_s is the squint angle, V_1 and V_2 are the amplitudes of the signals from sources A_1 and A_2, ω_1 and ω_2 are the frequencies of the signals from the two sources. The inputs to the sum and difference channels are:

$$v_{sum} = V_1(g(\theta_1 - \theta_s) + g(\theta_1 + \theta_s)) \cos \omega_1 t + V_2(g(\theta_2 - \theta_s) + g(\theta_2 + \theta_s)) \cos \omega_2 t$$

$$v_{dif} = V_1(g(\theta_1 - \theta_s) - g(\theta_1 + \theta_s)) \cos \omega_1 t + V_2(g(\theta_2 - \theta_s) - g(\theta_2 + \theta_s)) \cos \omega_2 t$$

At the output of the I-F amplifier, the signals are:

$$v_{IF,s} = K_{IF}(V_1(g(\theta_1 - \theta_s) + g(\theta_1 + \theta_s)) \cos \omega_{IF1} t + V_2(g(\theta_2 - \theta_s) + g(\theta_2 + \theta_s)) \cos \omega_{IF2} t)$$

$$v_{IF,d} = K_{IF}(V_1(g(\theta_1 - \theta_s) - g(\theta_1 + \theta_s)) \cos \omega_{IF1} t + V_2(g(\theta_2 - \theta_s) - g(\theta_2 + \theta_s)) \cos \omega_{IF2} t)$$

where the gains of the sum and difference channels are assumed to be the same and equal to K_{IF}; ω_{IF1} and ω_{IF2} are the intermediate frequencies of the two signals. The phase detector takes the average value of the product of $v_{IF,s}$ and $v_{IF,d}$. At the output of the phase detector, we have:

$$v_{pd} = K_{pd}(V_1^2(g^2(\theta_1 - \theta_s) - g^2(\theta_1 + \theta_s)) + V_2^2(g^2(\theta_2 - \theta_s) - g^2(\theta_2 + \theta_s)))$$

where K_{pd} is the phase detector constant.

Target A_1 will be used as a point of reference, and the angle θ will be measured from this point. This gives:

$$\theta_1 = \theta$$

$$\theta_2 = \theta - \Delta\theta$$

Defining $\zeta = V_1/V_2$ gives:

$$v_{pd} = K_{pd}(\zeta^2(g^2(\theta-\theta_s)-g^2(\theta+\theta_s))+(g^2(\theta-\Delta\theta-\theta_s)-g^2(\theta-\Delta\theta+\theta_s))) \tag{A-1}$$

Setting $v_{pd}=0$ in Equation (A-1) gives:

$$\zeta^2(g^2(\theta-\theta_s) - g^2(\theta+\theta_s)) = -(g^2(\theta-\theta_s-\Delta\theta) - g^2(\theta+\theta_s-\Delta\theta))$$

or,

$$\zeta^2 g^2(\theta-\theta_s) + g^2(\theta-\theta_s-\Delta\theta) = \zeta^2 g^2(\theta+\theta_s)+g^2(\theta+\theta_s-\Delta\theta) \tag{A-2}$$

For a Gaussian antenna pattern:

$$g(\theta) = g_o \exp(-2\ln2\,(\theta/\theta_{3m})^2)$$

$$g^2(\theta\pm\theta_s) = g_o^2 \exp(-4\ln2\,((\theta^2\pm2\theta\theta_s+\theta_s^2)/\theta_{3m}^2))$$

$$g^2(\theta\pm\theta_s-\Delta\theta) = g_o^2\exp(-4\ln2((\theta^2+\Delta\theta^2+\theta_s^2-2(\theta\pm\theta_s)\Delta\theta\pm2\theta\theta_s)/\theta_{3m}^2))$$

Substituting these values into Equation (A-2) above, and eliminating the common factors of g_o^2 and $\exp(-4\ln2\,(\theta^2+\theta_s^2)/\theta_{3m}^2)$, we have:

$$\zeta^2\exp(-4\ln2\,(-2\theta\theta_s/\theta_{3m}^2) + \exp(-4\ln2\,(\Delta\theta^2-2(\theta-\theta_s)\Delta\theta-2\theta\theta_s)/\theta_{3m}^2)$$

$$= \zeta^2\exp(-4\ln2\,(2\theta\theta_s/\theta_{3m}^2) + \exp(-4\ln2\,(\Delta\theta^2-2(\theta+\theta_s)\Delta\theta+2\theta\theta_s)/\theta_{3m}^2)$$

Re-arranging terms gives:

$$\exp(8\ln2\,\theta\theta_s/\theta_{3m}^2)\,(\zeta^2+\exp(-4\ln2\,(\Delta\theta^2-2(\theta-\theta_s)\Delta\theta)/\theta_{3m}^2)$$

$$= \exp(-8\ln2\,\theta\theta_s/\theta_{3m}^2)\,(\zeta^2+\exp(-4\ln2\,(\Delta\theta^2-2(\theta+\theta_s)\Delta\theta)/\theta_{3m}^2)$$

$$\frac{\zeta^2+\exp(-4\ln2\,(\Delta\theta^2-2(\theta-\theta_s)\Delta\theta)/\theta_{3m}^2}{\zeta^2+\exp(-4\ln2\,(\Delta\theta^2-2(\theta+\theta_s)\Delta\theta)/\theta_{3m}^2} = \exp(-16\ln2\,\theta\theta_s/\theta_{3m}^2)$$

$$\frac{\zeta^2+\exp(-4\ln2\,((\Delta\theta^2/\theta_{3m}^2)-2(\theta/\theta_{3m})(\Delta\theta/\theta_{3m})))\exp(-8\ln2\,(\theta_s/\theta_{3m})(\Delta\theta/\theta_{3m}))}{\zeta^2+\exp(-4\ln2\,((\Delta\theta^2/\theta_{3m}^2)-2(\theta/\theta_{3m})(\Delta\theta/\theta_{3m})))\exp(8\ln2\,(\theta_s/\theta_{3m})(\Delta\theta/\theta_{3m}))}$$

$$= \exp(-16\ln2\,\theta\theta_s/\theta_{3m}^2) \tag{A-3}$$

This transcendental equation will be used to solve for angular error ($\theta / \Delta \theta$) vs. the system parameters built into ζ^2 (the System J/S and the jammer antenna sidelobe levels).

Appendix B

Derivation of Power Ratio (ζ^2)

Equations (3) and (4) of Section II are derived in this Appendix.

It is assumed that the target aircraft is illuminated by a radar at range R_{ra} and the return signal is received by a semi-active missile at range R_{ma}. (See Figure 1) The power received at the missile due to the target is given by:

$$P_{rt} = \frac{P_r G_{ra}}{4\pi R_{ra}^2} \quad \frac{\sigma_t}{4\pi R_{ma}^2} \quad \frac{\lambda^2}{4\pi} \quad G_{ma} \tag{B-1}$$

where

    P_r = power of radar

    G_{ma} = gain of missile in direction of aircraft

    G_{ra} = gain of radar in direction of aircraft

    σ_t = target cross section

If the target aircraft offsets the received signal in Doppler, and re-transmits it toward the ground (with part of the signal returning directly to the missile), the power received by the missile due to the target aircraft becomes:

$$P_{rt} = \frac{P_r G_{ra}}{4\pi R_{ra}^2} \left(\frac{\sigma_t}{4\pi R_{ma}^2} + \frac{\lambda^2 G_{jr}}{4\pi} \quad \frac{G_r G_{jm}}{4\pi R_{ma}^2} \right) \frac{\lambda^2 G_{ma}}{4\pi} \tag{B-2}$$

where

    G_{jm} = gain of jammer in direction of missile

    G_{jr} = gain of jammer in direction of radar

    G_r = gain of repeater

81

It will be assumed that the illuminated ground patch may be replaced by a point source located below the ground (Figure 2-b), and that the reflection from the ground may be represented by a constant reflection coefficient times the signal incident upon the ground. Thus, the power received by the missile due to the false target (at range $R_{rf} \approx R_{ra}$) is given by:

$$P_{rf} = \frac{P_r G_{ra}}{4 \pi R_{ra}^2} \quad \frac{\lambda^2 G_{jr}}{4 \pi} \quad \frac{G_{jg} G_r \rho^2}{4 \pi R_{mf}^2} \quad \frac{\lambda^2 G_{mg}}{4 \pi} \tag{B-3}$$

where

$\quad G_{jg}$ = gain of jammer in direction of ground

$\quad G_{mg}$ = gain of missile in direction of ground

$\quad R_{mf}$ = distance from missile to false target

$\quad \rho^2$ = reflection parameter

The effective Jamming to Signal ratio is given by the ratio of received powers (Equation (B-2) divided by Equation (B-3):

$$\zeta^2 = \left(\frac{v_1}{v_2}\right)^2 = \frac{(1/4 \pi R_{ma}^2)(\sigma_t + (\lambda^2 G_{jm} G_r G_{jr}/4 \pi)) G_{ma}}{(\lambda^2 G_{jr}/4 \pi)(G_{jg} \rho^2/(4 \pi R_{mf}^2)) G_{mg}} \tag{B-4}$$

It is assumed that $G_{ma} = G_{mg}$ as long as both the target and the ground patch are within the missile's 3-dB beamwidth. Thus,

$$\zeta^2 = \left(\frac{R_{mf}}{R_{ma}}\right)^2 \left(\frac{\sigma_t + (\lambda^2/4 \pi) G_r G_{jm} G_{jr}}{(\lambda^2/4 \pi) G_r G_{jg} G_{jr} \rho^2}\right) \tag{B-5}$$

82

The System Jamming to Signal Ratio $(J/S)_s$ is given by:

$$(J/S)_s = \frac{\lambda^2 G_{jr} G_r G_{jg}/(4\pi 4\pi R_{ma}^2)}{\sigma_t/(4\pi R_{ma}^2)} = \frac{(\lambda^2/4\pi)G_{jg}G_r G_{jr}}{\sigma_t} \qquad (B-6)$$

Derivation of Doppler Offset of Reflected Signal from Direct Path Signal

Equation (8) of Section II is derived in this Appendix.

Figure 7 shows the overall system geometry for the problem. From Figure 7 we have:

$$R_{ga} = H_t / \sin \psi_t \tag{C-1}$$

$$R_{mg} = H_r / \sin \psi_r \tag{C-2}$$

$$R_{ma} = R / \cos \theta_{ma} \tag{C-3}$$

Figure C-1a indicates the geometry of the velocity vectors of the missile and aircraft. ψ is the angle between $\vec{v}_a$ and $\hat{x}_{ma}$ (the line of sight between the aircraft and the missile). ϕ, the angle between $\vec{v}_m$ and $-\hat{x}_{ma}$, must be determined in terms of ψ. R_{ma}, R_{ai}, and R_{mi} are the ranges between the missile and the aircraft; the aircraft and the projected point of intercept; and the missile and the projected point of intercept. R and R'_{mi} are the ground projections of R_{ma} and R_{mi}. Assuming that $\vec{v}_m$ and $\vec{v}_a$ are constant, we have:

$$t = R_{ai}/v_a = R_{mi}/v_m \tag{C-4}$$

where t is the time to intercept. This gives:

$$R_{ai} = (v_a/v_m)R_{mi} \tag{C-5}$$

From trigonometry:

$$R_{ma}/\sin(180° - \phi - \psi) = R_{ai}/\sin\phi = R_{mi}/\sin\psi \tag{C-6}$$

84

Equations (C-5) and (C-6) give:

$$R_{ai} = R_{ma} \sin \phi / \sin(180° - \phi - \psi) = (v_a/v_m) R_{ma} \sin \psi / \sin(180° - \phi - \psi)$$

$$\sin \phi = (v_a/v_m) \sin \psi$$

$$\phi = \sin^{-1}((v_a/v_m) \sin \psi) \tag{C-7}$$

Figure C-1b shows the geometry of $\vec{v}_a$ and $\hat{x}_{ga}$ (the path from the aircraft to the ground). A triangle is formed by sides R_{ai}, R_{ga}, and R_{gi}. R'_{ai}, x_1, and R'_{gi} are the ground projections of these sides. η is the angle between $\vec{v}_a$ and $\hat{x}_{ga}$, and may be found from:

$$R_{gi}^2 = R_{ai}^2 + R_{ga}^2 - 2 R_{ai} R_{ga} \cos \eta \tag{C-8}$$

where $R'_{ai} = R_{ai}$ (assuming that the aircraft is in level flight), and R_{ga} is given by Equation (C-1). R_{gi} may be found from:

$$R_{gi}^2 = H_t^2 + R'^2_{gi} \tag{C-9}$$

R'_{gi} may be found from Figure C-1b:

$$R'^2_{gi} = R'^2_{ai} + x_1^2 - 2 x_1 R'_{ai} \cos \psi' \tag{C-10}$$
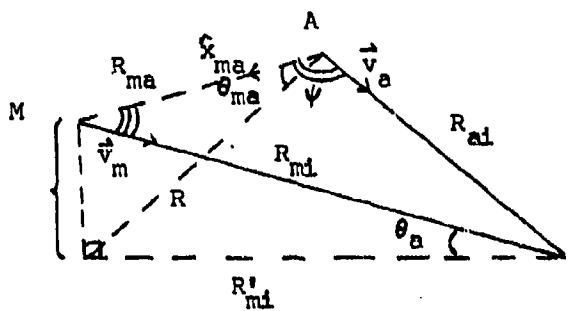
From Figure C-1a:

$$\cos \psi' = \frac{R_{ai}^2 + R^2 - R_{mi}^2 \cos \theta_a}{2 R R_{ai}} \tag{C-11}$$
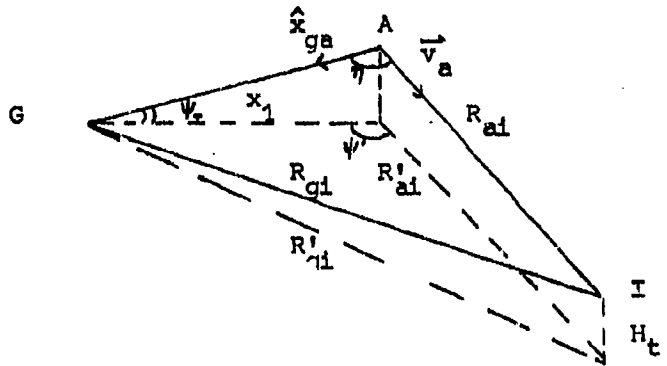
$$\theta_a = \sin^{-1}((H_r - H_t)/R_{mi}) = \sin^{-1}(R \tan \theta_{ma}/R_{mi}) \tag{C-12}$$

R_{mi} is found from:
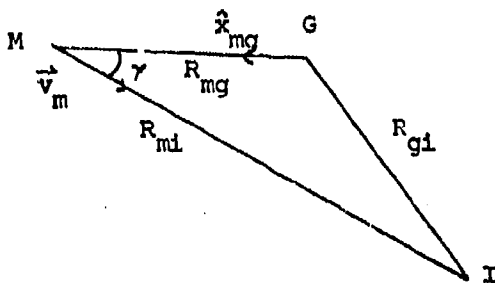
$$R_{mi} = (v_m/v_a) R_{ai} = R_{ma} \sin \psi / \sin(180° - \phi - \psi) \tag{C-13}$$

85

(a) Geometry of $\hat{x}_{ma}$, $\vec{v}_a$, and $\vec{v}_m$

(b) Geometry of $\hat{x}_{ga}$ and $\vec{v}_a$

(c) Geometry of $\hat{x}_{mg}$ and $\vec{v}_m$

Figure C-1. Identification of Angles in Reflection Geometry

Using Equations (C-12) and (C-13) in Equations (C-11) and (C-10), we have:

$$R_{gi}^2 = R_{ai}^2 + x_1^2 - (x_1/R)(R_{ai}^2 + R^2 - R_{mi}^2 Cos^2 \theta_a) \qquad (C-14)$$

Using Equation (C-14) in Equation (C-9) gives:

$$R_{gi}^2 = H_t^2 + R_{ai}^2 + x_1^2 - (x_1/R)(R_{ai}^2 + R^2 - R_{mi}^2 Cos^2 \theta_{ma}) \qquad (C-15)$$

Using Equations (C-15) and (C-1) in Equation (C-8) gives:

$$\eta = Cos^{-1}\left(\frac{R_{ai}^2 + R_{ga}^2 - R_{gi}^2}{2 R_{ai} R_{ga}}\right) \qquad (C-16)$$

Figure C-1c shows the geometry of $\vec{v}_m$ and $\hat{x}_{mg}$ (the path from the ground to the missile). γ is the angle between $\vec{v}_m$ and $-\hat{x}_{mg}$. A triangle is formed by R_{mg}, R_{mi}, and R_{gi}, defined in Equations (C-2), (C-13), and (C-15). γ may be determined from:

$$R_{gi}^2 = R_{mi}^2 + R_{mg}^2 - 2 R_{mi}R_{mg} Cos \gamma$$

$$\gamma = Cos^{-1}\left(\frac{R_{mi}^2 + R_{mg}^2 - R_{gi}^2}{2 R_{mi}R_{mg}}\right) \qquad (C-17)$$

87
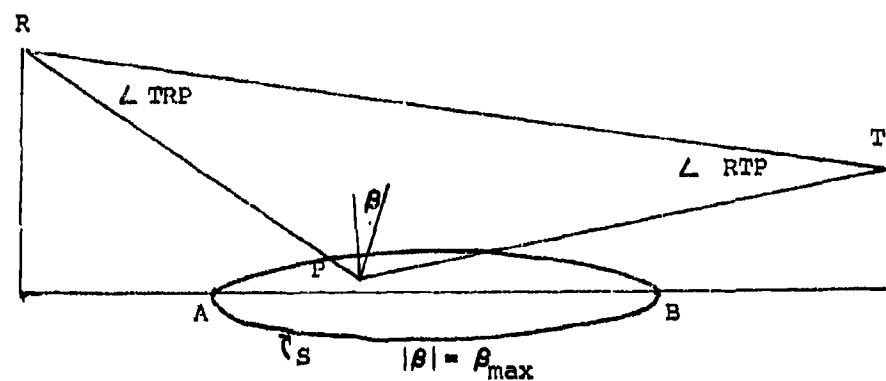
Appendix D

Derivation of Equation for Glistening Area

Equation (14) of Section II is derived in this Appendix (Reference 7: Chapter 12). Figure D-1 shows the geometry of the problem. Antennas at the transmitter (T) and the receiver (R) are at heights H_t and H_r and separation R. The antennas illuminate an area between them. For omnidirectional antennas, the region of the surface for which $|\beta| \leq \beta_{max}$ participates in reflection. The contour S bounds this "glistening area". P is an arbitrary point on the surface bounded by S. $\angle$ RTP and $\angle$ TRP are maximum at the points A and B where the curve $|\beta| = \beta_{max}$ intersects the vertical plane passing through R and T. The angle made by the bisector with the vertical (z-axis) is defined as β. The bisectors of $\angle$ TAR and $\angle$ TBR make angles β_{max} from the vertical. (This comes from the assumption of specular reflection from a mirror of slope Tan β_{max}. See Figure 10.) Thus, $|\beta| = \beta_{max}$ at the boundary of the contour.
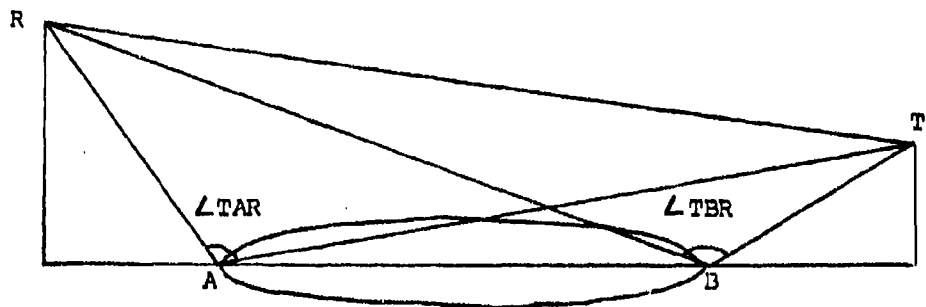
x_1 is the distance along the x-axis from the base of the receiver to P; x_2 is the distance from P to the base of the transmitter; $x_1 + x_2 = R$; and y is the distance of P from the x-axis. The boundary of the glistening area is determined by finding β in terms of x_1, x_2, and y, and setting $|\beta| = \beta_{max}$.

Figure D-1c indicates the geometry of the reflection problem. It is necessary to find angle β, the angle between the bisector $\hat{c}$ and the vertical $\hat{z}$. From Figure D-1c, the bisector of $\overrightarrow{RP}$ and $\overrightarrow{PT}$ is given by:
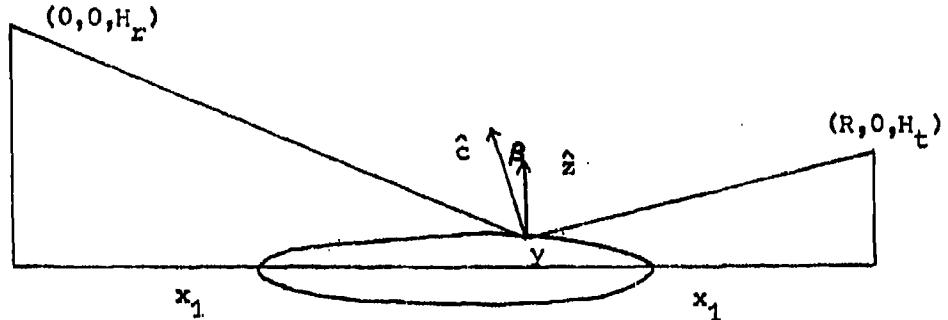
$$\hat{c} = \frac{\widehat{PR} + \widehat{PT}}{|\widehat{PR} + \widehat{PT}|} \tag{D-1}$$

(a) The glistening area is bounded by the contour S $(|\beta| = \beta_{max})$.

(b) A point (P) on the glistening area reflects a signal from T to R. β is the angle made by the bisector of the incident and receive angles with the normal.

(c) Geometry used to determine β at a point on the glistening area.

Figure D-1. Glistening Area Geometry

where ($\rightarrow$) denotes a vector quantity, and ($\wedge$) denotes a unit vector.

From Figure D-1c:

$$\overline{PR} = (0\,\hat{x} + 0\,\hat{y} + H_r\hat{z}) - (x_1\hat{x} \pm y\,\hat{y} + 0\,\hat{z}) = -x_1\,\hat{x} \mp y\,\hat{y} + H_r\hat{z}$$

$$\overline{PT} = (R\,\hat{x} + 0\,\hat{y} + H_t\hat{z}) - (x_1\hat{x} \pm y\,\hat{y} + 0\,\hat{z}) = x_2\,\hat{x} \mp y\,\hat{y} + H_t\hat{z}$$

where $x_2 = R - x_1$. This gives:

$$\hat{PR} = (1/a_1)(-x_1\hat{x} \mp y\,\hat{y} + H_r\hat{z})$$

$$\hat{PT} = (1/a_2)(x_2\hat{x} \mp y\,\hat{y} + H_t\hat{z})$$

where

$$a_1 = \sqrt{x_1^2 + y^2 + H_r^2}$$

$$a_2 = \sqrt{x_2^2 + y^2 + H_t^2}$$

This gives:

$$\hat{PR} + \hat{PT} = \left(\frac{-x_1}{a_1} + \frac{x_2}{a_2}\right)\hat{x} \mp \left(\frac{y}{a_1} + \frac{y}{a_2}\right)\hat{y} + \left(\frac{H_r}{a_1} + \frac{H_t}{a_2}\right)\hat{z}$$

$$\hat{PR} + \hat{PT} = \sqrt{\left(\frac{x_1^2 + y^2 + H_r^2}{a_1^2}\right) + \left(\frac{x_2^2 + y^2 + H_t^2}{a_2^2}\right) + \left(\frac{-2x_1x_2 + 2y^2 + 2H_rH_t}{a_1a_2}\right)}$$

$$= \sqrt{2 + 2\left(\frac{-x_1x_2 + y^2 + H_rH_t}{a_1a_2}\right)} = b$$

Thus, the bisector is given by:

$$\hat{c} = \frac{\hat{PR} + \hat{PT}}{|\hat{PR} + \hat{PT}|} = \frac{1}{b}\left(\frac{-x_1}{a_1} + \frac{x_2}{a_2}\right)\hat{x} + \frac{1}{b}\left(\frac{y}{a_1} + \frac{y}{a_2}\right)\hat{y} + \frac{1}{b}\left(\frac{H_r}{a_1} + \frac{H_t}{a_2}\right)\hat{z}$$

Using the definition of β, ($\cos \beta = \hat{c} \cdot \hat{z}$), and setting $|\beta| = \beta_{max}$ at the boundary of the glistening area, we have:

$$\cos \beta = \hat{c} \cdot \hat{z} = \frac{1}{b} \left(\frac{H_r}{a_1} + \frac{H_t}{a_2} \right) \qquad (D-2)$$

VITA

Nancy C. Strasser, (née Taylor) was born on 9 December 1953 in Baltimore, Maryland. Her parents are William C. Taylor and Mary Smith Taylor of Baltimore. She graduated Cum Laude from Loyola College, Baltimore, with a Bachelor of Science Degree in Physics. She was commissioned in the U.S. Air Force through the Officers Training School in San Antonio, Texas. Captain Strasser was assigned to the Foreign Technology Division (Air Force Systems Command) from January 1976 to October 1979. She is a recipient of the Air Force Commendation Medal.

Permanent Address: 2202 Mayfield Avenue

Baltimore, Maryland 21213

REPORT DOCUMENTATION PAGE	READ INSTRUCTIONS BEFORE COMPLETING FORM	
1. REPORT NUMBER AFIT/GE/EE/80D-41	2. GOVT ACCESSION NO. AD-A101 208	3. RECIPIENT'S CATALOG NUMBER
4. TITLE (and Subtitle) INVESTIGATION OF TERRAIN BOUNCE ELECTRONIC COUNTERMEASURE		5. TYPE OF REPORT & PERIOD COVERED MS Thesis
		6. PERFORMING ORG. REPORT NUMBER
7. AUTHOR(s) Nancy C. Strasser Captain		8. CONTRACT OR GRANT NUMBER(s)
9. PERFORMING ORGANIZATION NAME AND ADDRESS Air Force Institute of Technology (AFIT-EN) Wright-Patterson AFB, Ohio 45433		10. PROGRAM ELEMENT, PROJECT, TASK AREA & WORK UNIT NUMBERS
11. CONTROLLING OFFICE NAME AND ADDRESS Air Force Wright Aeronautical Labs AFWAL/AAWW Wright Patterson AFB, Ohio 45433		12. REPORT DATE December, 1980
		13. NUMBER OF PAGES 104
14. MONITORING AGENCY NAME & ADDRESS(if different from Controlling Office)		15. SECURITY CLASS. (of this report) Unclassified
		15a. DECLASSIFICATION/DOWNGRADING SCHEDULE

16. DISTRIBUTION STATEMENT (of this Report)

Approved for public release; distribution unlimited

17. DISTRIBUTION STATEMENT (of the abstract entered in Block 20, if different from Report)

18. SUPPLEMENTARY NOTES

16 JUN 1981

Approved for public release; IAW AFR 190-17

Frederic C. Lynch, Major, USAF
Director of Public Affairs

19. KEY WORDS (Continue on reverse side if necessary and identify by block number)

Terrain Bounce
Reflection, Reflectivity
Electronic Countermeasure, ECM
Scattering

20. ABSTRACT (Continue on reverse side if necessary and identify by block number)

"Terrain Bounce" is an electronic countermeasure intended to defeat Amplitude Comparison Monopulse Tracking. In this paper the countermeasure technique is described and its theoretical basis is developed. The two-target tracking problem, the Doppler offset and spreading of the ground-reflected signal, and a model for reflection from rough terrain are presented. A methodology is developed for analyzing the Terrain Bounce problem. The theory is applied to a typical Terrain Bounce geometry, and the resulting jammer requirements are derived.

DD FORM 1473 EDITION OF 1 NOV 65 IS OBSOLETE